ELECTRODELESS TECHNIQUES FOR SEMICONDUCTOR MEASUREMENTS

and

DIMORPHIC PHASE TRANSFORMATIONS IN COMPOUND SEMICONDUCTORS

by

DONALD WALTER NYBERG

B. A. Sc., University of British Columbia, 1957

A THESIS SUBMITTED IN PARTIAL FULFILMENT OF

THE REQUIREMENTS FOR THE DEGREE OF

MASTER OF APPLIED SCIENCE

in the Department

of

Physics

We accept this thesis as conforming to the

required standard

THE UNIVERSITY OF BRITISH COLUMBIA

April, 1960

In presenting this thesis in partial fulfilment of the requirements for an advanced degree at the University of British Columbia, I agree that the Library shall make it freely available for reference and study. I further agree that permission for extensive copying of this thesis for scholarly purposes may be granted by the Head of my Department or by his representatives. It is understood that copying or publication of this thesis for financial gain shall not be allowed without my written permission.

Department of Physics

The University of British Columbia,
Vancouver 8, Canada.

Date April 7, 1960

ABSTRACT

Electrodeless techniques for semiconductor measurements, based on the inductive coupling of the sample to coils, are investigated in the first part of the thesis. The theory and the experimental techniques of two main experiments are developed and applied to several samples. The second part of the thesis is devoted to discussing dimorphic phase transformations in compound semiconductors.

In the first experiment the sample is placed in the core of a solenoid which is excited by a sine wave generator. Eddy currents are induced in the sample and they set up a secondary magnetic field which opposes the primary field resulting in a decrease in flux through the core. The result is that a complex impedance is reflected into the coil. The increase in resistance and decrease in inductance of the coil is measured by a Q-meter technique and related to the conductivity for long cylindrical and spherical geometry samples. Design considerations are discussed, and it is shown that the optimum frequency to use, in order to obtain maximum sensitivity with the Q-meter, will depend on the conductivity of the material. Longitudinal and transverse magnetoresistance are observed by applying a static magnetic field along the appropriate axis of the solenoid.

The second experiment is a crossed magnetic field determination of the Hall mobility. Circulating eddy currents are induced in the sample by a sinusoidally excited coil and a static magnetic field is applied along a second axis. The static field will rotate the plane of the eddy currents through the Hall angle, $u_H B$, the product of the Hall mobility and the

static field. The effect is the appearance of an alternating magnetic field along the third axis. This field, which at low frequencies is directly proportional to the Hall mobility, is detected by a second coil. The technique is very general and it is independent of the conductivity. In particular, it may be used to determine the Hall mobility of powders and liquids to which it is difficult or impossible to attach electrodes.

In the second part of the thesis the compound semiconductor silver selenide is investigated. The sample could be obtained commercially only in powder form and hence the electrodeless techniques were essential. The temperature variation of conductivity above and below the phase transition, activation energies, relative conductivities at the phase transition and a conductivity-temperature hysteresis effect were observed. Absolute conductivity values were not obtained because of lack of knowledge of the radii of the individual powder grains and the Hall mobility measurements indicated that the sample was very impure, electronically speaking, and hence only impurity scattering was being measured.

TABLE OF CONTENTS

PART I: ELECTRODELESS TECHNIQUES FOR SEMICONDUCTOR MEASUREMENTS

PART II: DIMORPHIC PHASE TRANSFORMATIONS IN COMPOUND SEMICONDUCTORS

LIST OF FIGURES

A C K N O W L E D G M E N T S

I wish to thank Professor R. E. Burgess for his guidance throughout the course of this work, and for his valuable comments and constructive criticism during the preparation of this thesis.

The assistance of the National Research Council of Canada through a Postgraduate Studentship, Bursary and Summer Supplement is gratefully acknowledged.

I also wish to acknowledge the assistance of the Defense Research Board in providing many of the research facilities used in this work.

PART I: ELECTRODELESS TECHNIQUES FOR SEMICONDUCTOR MEASUREMENTS

CHAPTER 1 - INTRODUCTION

Electrodeless techniques for determining the electrical conductivity, magnetoresistance effect, and Hall mobility of a semiconductor will be described. The techniques are based on inductive coupling of the sample to coils and have several advantages over the standard 4-electrode techniques. In particular, samples to which it would be difficult to attach electrodes, such as liquids and chemically active substances which might need to be kept in a vacuum, inert gas atmosphere, or under pressure may be studied while in a suitable container, provided the container is an insulator. Another important class of materials to which electrodes may not be attached are powders. They are frequently the initial product in the chemical preparation of a new material. It will be shown in part II that, although absolute conductivities are not obtainable by the electrodeless technique, relative conductivities at phase changes, temperature variation of conductivities, activation energies, and Hall mobilities are readily measured for powders. In addition, the problem of making ohmic contacts, although partly overcome by 4-electrode techniques, is completely eliminated by these techniques.

The electrical conductivity of a sample is determined by placing the sample in the core of a solenoid. The solenoid is excited by a sine wave generator, eddy currents are induced in the sample, and the secondary magnetic field set up by the eddy currents opposes the exciting field resulting in an attenuation of the field as it penetrates into the sample. The eddy currents flowing in the lossy material result in a power loss

which is reflected into the solenoid as an increase in resistance. The attenuation of the magnetic field inside the sample results in a decrease in flux through the solenoid core and hence is reflected into the solenoid as a decrease in inductance. These resistance and inductance changes are measured by a Q-meter technique and are readily related to the conductivity of the material for specific sample geometries.

Busch, Wieland and Zoller (1951) have studied the electrical conductivity of grey tin as a function of temperature using these techniques. The Q-factor of a coil containing a core of grey tin powder was measured at frequencies up to 30 Mc. In particular,

$$\sigma(T) = K\left(\frac{1}{Q_1} - \frac{1}{Q_0}\right).$$

where K = a constant dependent on frequency, geometrical shape and dimensions of the conducting particles, but independent of temperature,

Q_1 = Q-factor of the coil with sample inside,

and Q_0 = Q-factor of the coil without the sample.

The experimenters took care to ensure that during the experiment no change of particle size, due to agglomeration, or due to crumbling of individual grains of the powder, took place. The constant K was not known due to uncertainty as to the size of the powder grains, however, since K is independent of temperature, σ/K can be measured as a function of temperature.

In general it is not possible to obtain absolute conductivity values for powders because K cannot be determined. However, in this particular case K was obtained approximately by a comparison method. The Q-factor, Q_α of the coil was measured for grey tin (α-tin), then the sample was heated, allowed to revert back to white tin (β-tin) and the Q-factor, Q_β

was measured at the same temperature as that of the grey tin. The conductivity of white tin is known by other methods, hence

$$\frac{\sigma_\alpha}{\sigma_\beta} = \left(\frac{Q_o - Q_\alpha}{Q_o - Q_\beta} \right) \frac{Q_\beta}{Q_\alpha}$$

The results must be corrected for a decrease in volume of 21% in the $\alpha \rightarrow \beta$ transition.

The Hall mobility of a semiconductor is determined by a crossed magnetic field technique. Eddy currents are induced in the sample by an alternating magnetic field. The eddy currents flow solenoidally, in a plane perpendicular to the direction of the applied magnetic field. A static magnetic field applied parallel to the plane of the eddy currents causes the plane of the eddy currents to rotate about the axis of the static field through an angle which is proportional to the product of μ_H the Hall mobility and to B, the static magnetic field. The secondary magnetic field set up by the eddy currents perpendicular to their plane will also be rotated through this angle, the effect being an alternating magnetic field along the third axis, perpendicular to both the exciting and static magnetic fields, and proportional to the Hall mobility. A coil with center line along this axis will detect a voltage which is proportional to the Hall mobility. In the experimental technique developed, a pair of Helmholtz coils is used to provide the exciting field and a solenoid is the detecting coil. The coils are mounted between the poles of a dc magnet.

This electrodeless technique for making Hall mobility measurements on semiconductors is beleived to be new and it should prove to be a useful experimental technique because of its advantages over conventional techniques requiring electrodes. In addition to the advantages listed under

the description of the conductivity experiment, this technique has the very important advantage, which will be discussed further in part II, in that it is the only known general method of obtaining absolute Hall mobility measurements on powders. The reason that the method is valid for powders is that at low frequencies the results are essentially independent of the conductivity and the shape and size of the sample but are proportional to the rotation of the plane of the eddy currents which is itself proportional only to the product $u_H B$. Busch, Wieland and Zoller (1951) have used dc methods on powders to obtain u_H, but two experimental difficulties are that the current must flow across particle boundaries, and the current density is not easily defined due to incomplete packing of the granular structure. The electrodeless technique overcomes both of these difficulties.

Busch, Jaggi and Braunschweig (1953) have described a two electrode technique for making measurements of Hall mobilities. In particular, consider a sample of conductivity σ, in the shape of a thin circular disc. A simusoidally varying magnetic field $B = B_0 \sin\omega t$ perpendicular to the plane of the disc will set up circulating eddy currents in the disc. The tangential electric field and current density are,

$$E_\phi = -\frac{\omega r}{2} B_0 \cos \omega t$$

and

$$J_\phi = -\frac{\omega \sigma r}{2} B_0 \cos \omega t$$

The magnetic field will also exert a radial force on the current carriers. The radial force on an electron is,

$$-eE_r = -e|\vec{v} \times \vec{B}|$$

If the charge density is n, then

$$n e E_r = n e v_\phi B_z$$

$$= J_\phi B_z$$

$$= \frac{\omega \sigma r}{2} B_o^2 \cos \omega t \sin \omega t .$$

Substituting for J_ϕ, and using $\sigma = neu$,

$$E_r = \frac{u \omega r}{2} B_o^2 \cos \omega t \sin \omega t$$

$$= \frac{u \omega r}{4} B_o^2 \sin 2\omega t .$$

Since no current can flow in the radial direction, a potential V_r will appear between the center and the rim of the disc. If r_o, is the radius of the disc, then

$$V_r = \frac{u \omega r_o^2}{8} B_o^2 \sin 2\omega t .$$

Hence

$$u = \frac{8 V_r}{\omega r_o^2 B_o^2 \sin 2\omega t} .$$

The major advantage of Busch's method is that the mobility is obtained independently of the conductivity. However, it is still necessary to attach two electrodes to the sample, and thus the method seems to offer little advantage over other techniques employing electrodes.

Materials with exceptionally high mobilities, such as indium antimonide, offer possibilities for obtaining additional information about the Hall mobility as the product $u_H B$ can be greater than unity and the phenomena of magnetoresistance is pronounced. In particular, the voltage on the detection coil in the Hall mobility experiment measured as a function of B will show a maximum at a value of $u_H B$ which is readily predicted theoretically. Hence the value of u_H is obtained in terms of the parameter B, and independently of frequency, geometry, size and conductivity.

In addition, various magnetoresistance experiments may be made using the technique described for determining conductivities. The resistance reflected into the solenoid as a function of B may be related theoretically to the product $u_{H}B$. Two particular experiments are described, one a transverse magnetoresistance experiment in which the static magnetic field is perpendicular to the plane of the eddy currents and a second in which the static magnetic field is parallel to the plane of the eddy currents. Measurements are made on a single crystal of indium antimonide and the results are compared with theory.

CHAPTER 2 - EXPERIMENTAL TECHNIQUES

2.1 Eddy Current Losses in a Solenoid Core

(a) General Techniques. The sample, assumed to be of uniform conductivity and permeability, is placed inside a solenoid. The solenoid must be longer than the sample so that the exciting magnetic field is uniform and axial. A simusoidal voltage generator is connected across the solenoid and the resistance and inductance changes reflected into the coil by the sample are measured by a Q-meter technique. The change in resistance is related to the conductivity of the material for two special cases in appendices A and B. Conductivities are measured as a function of temperature by placing the solenoid and sample in a temperature controlled oil bath.

The formulae for the change in resistance and inductance of a solenoid due to a long cylindrical sample of radius r_o and length l_o are given for the two limiting cases as:

(i) low frequency limit $(\omega\sigma\mu_o)^{\frac{1}{2}} r_o = br \leq \frac{1}{2}$,

$$\frac{\Delta R}{\omega L_o} = K_c \frac{(br_o)^2}{8}, \tag{A19}$$

and

$$\frac{\Delta L}{L_o} = -\frac{K_c (br_o)^4}{96}, \tag{A18}$$

where

$$K_c = \frac{r_o^2 l_o}{r_c^2 l_c}, \tag{A13}$$

and r_c = radius and l_c = length of solenoid.

(ii) high frequency limit $br_o \geq 10$,

$$\frac{\Delta R}{\omega L_o} = \frac{\sqrt{2}\, K_c}{br_o}, \tag{A22}$$

Facing Page 8

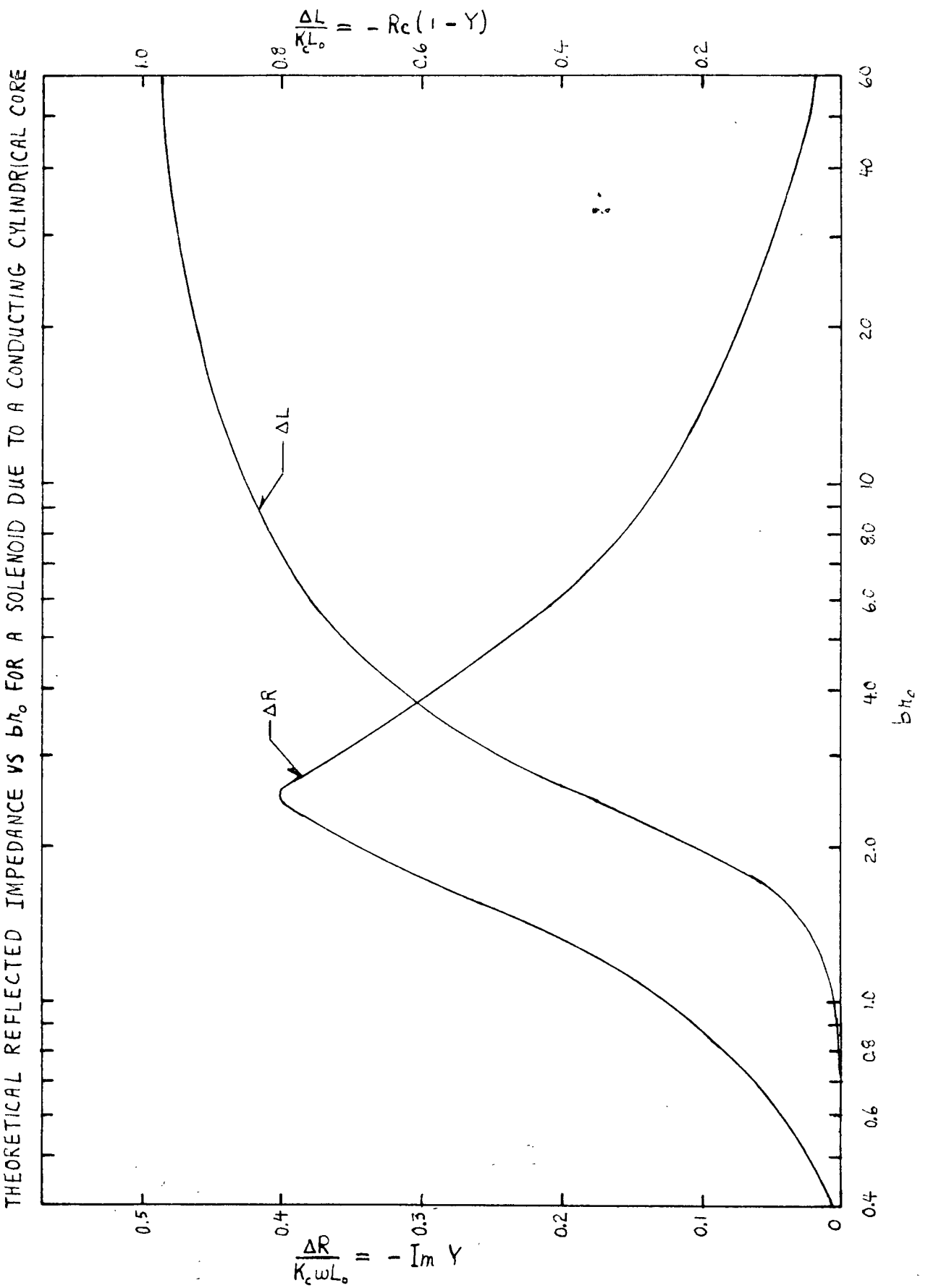

FIGURE 1

THEORETICAL REFLECTED IMPEDANCE VS $b h_o$ FOR A SOLENOID DUE TO A CONDUCTING CYLINDRICAL CORE

and $$\frac{\Delta L}{L_o} = -K_c\left(1 - \frac{\sqrt{2}}{br_o}\right). \qquad (A21)$$

The general formulae for $\Delta R/\omega L_o$ (A16) and $\Delta L/L_o$ (A15) as a function of br_o are plotted in Fig. 1.

The formulae for the change in resistance and inductance of a solenoid due to a spherical sample of radius r_o are given in the low frequency limit $br_o \leq \frac{1}{2}$ by:

$$\frac{\Delta R}{\omega L_o} = K_s \frac{(br_o)^2}{10}, \qquad (B7)$$

and $$\frac{\Delta L}{L_o} = -K_s \frac{(br_o)^4}{105}, \qquad (B6)$$

where $$K_s = \frac{4 r_o^3}{3 r_c^2 L_c} \qquad (B8)$$

(b) Measurement of ΔR and ΔL. The changes in resistance and inductance of the solenoid are measured with a Q-meter. Let L_o and R_o refer to the inductance and series resistance of the solenoid. Then $Q_o = \omega_o L_o/R_o$. Similarly let L_s, R_s and Q_s refer to the same quantities with the sample in place in the core. Then

$$\Delta R = R_s - R_o$$

$$= \omega_o L_o \left(\frac{1}{Q_s}\frac{L_s}{L_o} - \frac{1}{Q_o}\right) \qquad (1)$$

No commercial Q-meter of the necessary frequency range was available. Consequently an improvised Q-meter was designed. Two circuits, the parallel tuned and the series tuned, were considered:

(i) Parallel tuned (Fig. 2a)

Now $$I = \mathcal{E}\left(j\omega C + \frac{1}{R + j\omega L}\right),$$

hence $$\left|\frac{\mathcal{E}}{I}\right|^2 = \frac{R^2 + \omega^2 L^2}{(1-\omega^2 LC)^2 + (\omega C R)^2}.$$

Facing Page 9

FIGURE 2

Q-METER CIRCUITS

(a) PARALLEL TUNED Q-METER

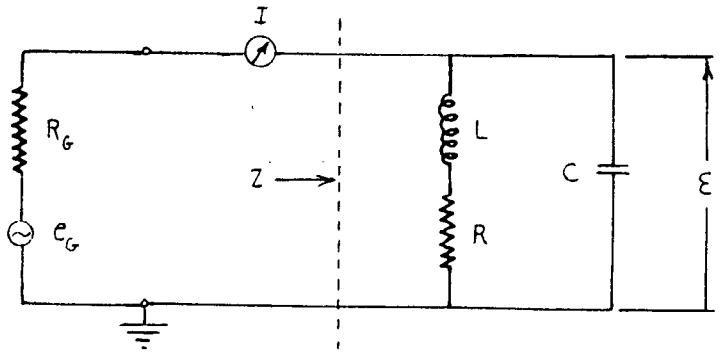

(b) SERIES TUNED Q-METER

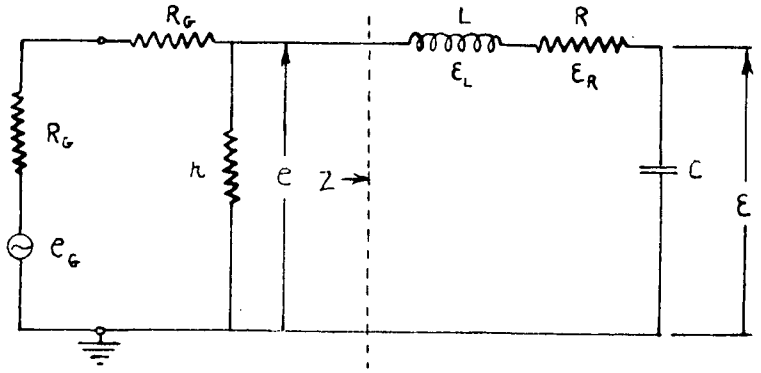

$r << R, R_G$

(c) SERIES TUNED Q-METER WITH SHUNT CAPACITANCE

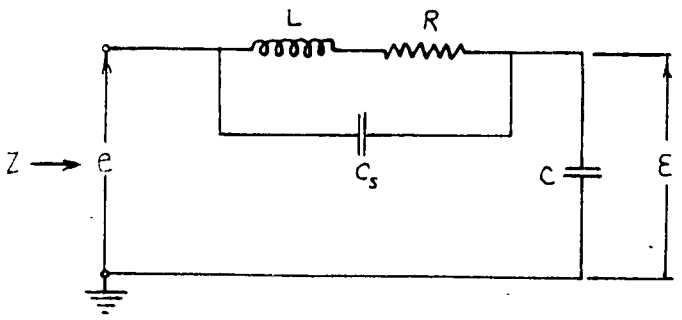

If $\left(\frac{\omega_0 L}{R}\right)^2 = Q^2 >> 1$, $\left|\frac{\mathcal{E}}{I}\right|$ has its maximum very close to the condition $\omega_0^2 LC = 1$.

Thus $$Q = \omega_0 C \left|\frac{\mathcal{E}}{I}\right|,$$

or $$Q = \frac{1}{\omega_0 L}\left|\frac{\mathcal{E}}{I}\right|. \qquad (2)$$

(ii) Series tuned (Fig. 2b)

At resonance, that is when $\omega_0^2 LC = 1$ and for $Q > 10$ say,

$$\mathcal{E}_c = -\mathcal{E}_L \text{ and } \mathcal{E}_R = e.$$

Hence $$Q = \frac{\omega_0 L}{R} = \frac{\mathcal{E}}{e}. \qquad (3)$$

A comparison of the two circuits shows that the input impedance of the parallel tuned circuit, $\omega_0 LQ$, may be quite high making it difficult to supply a constant current. If the current is not kept constant, I must be measured and this is difficult if no suitable ammeter is available. On the other hand, to supply a constant voltage to the series tuned circuit requires only that $r << R$. The series tuned circuit was chosen and in practice the constant voltage condition was not essential since e and $\mathcal{E}$ were easily measured with vacuum tube voltmeters.

The effect of the stray shunt capacitance C_s of the coil is to lower the apparent Q. Refer to Fig. 2c. The input impedance of the circuit,

$$Z = \frac{1}{j\omega C} + \frac{1}{j\omega C_s + \frac{1}{R + j\omega L}}$$

$$= \frac{1 - \omega^2 L(C + C_s) + j\omega R(C + C_s)}{j\omega C\{1 - \omega^2 L C_s + j\omega C_s R\}}.$$

Now $|Z|$ has a minimum very close to the condition $\omega_0^2 L(C + C_s) = 1$.

FIGURE 3

Q-METER CIRCUIT DIAGRAM

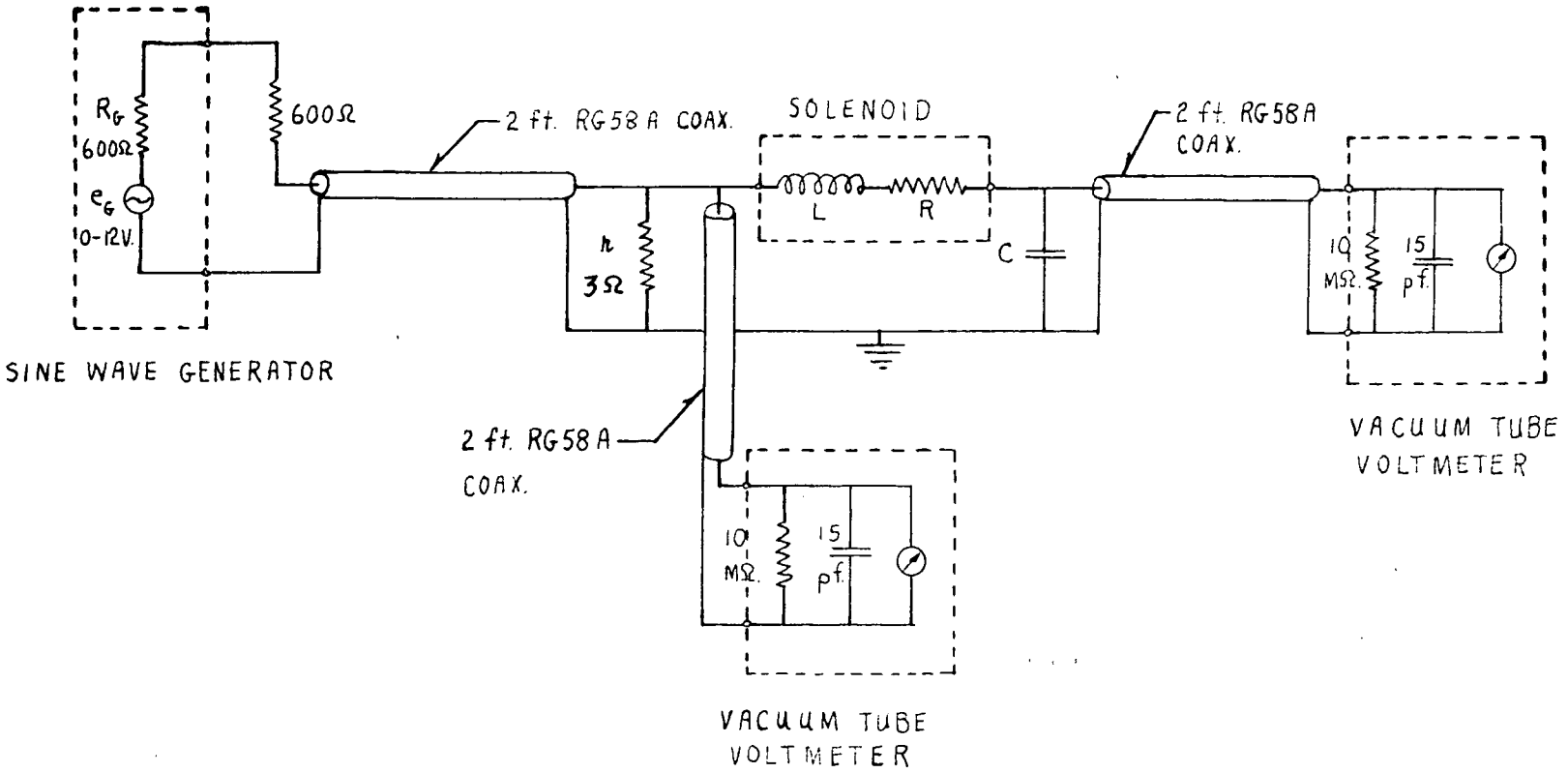

Hence $$Z = \frac{C + C_s}{C} \frac{1}{\omega_o^2 LC + j\omega C_s R}.$$

But $$\omega C_s R << \omega_o^2 LC,$$

thus $$\frac{\mathcal{E}}{e} = \frac{1}{j\omega_o C Z} = \frac{\omega_o L}{R} \frac{C}{C + C_s}.$$

Hence $$Q = \frac{\omega_o L}{R} = \frac{\mathcal{E}}{e} \frac{C + C_s}{C}.$$

The Q-meter was constructed as follows. A Shasta Model 301A sine wave generator and two Hewlett Packard Model 400D, vacuum tube voltmeters were connected as shown in Fig. 3. The values of the circuit elements are as shown. The frequency range available with this generator was 10 cps to 1 Mc. In fixing the values of the circuit elements it is desirable that certain conditions be met. First of all, $r << R$ makes e independent of R. Secondly, a frequency should be chosen so that the tuning capacitance C is large compared to C_s, the stray capacitance of the coil, and to the combined capacitance of the connecting cable and the internal capacitance of the vacuum tube voltmeter measuring $\mathcal{E}$. The minimum value of C, say $C_m = 500$ pf limits the maximum inductance of the coil. This point is considered in the next section. All leads are shielded to minimize the pickup of stray 60 cps radiation.

If ΔL is negligible, then C may be fixed at a convenient value and the frequency varied until resonance is obtained. However, if ΔL is non-zero, then C must be a calibrated variable capacitor so that the circuit may be retuned and ΔL measured when the sample is added.

(c) Design Considerations. The physical dimensions of the sample are usually fixed by practical considerations. The solenoid is then made slightly bigger so that the sample may be placed inside. The next questions one asks are what frequency should one use and what value of inductance should the coil have in order to obtain the maximum observable effect.

The first design criterion is that for good sensitivity one wishes $Q_s \leq Q_o/2$ say, where Q_s = Q of the coil with the sample and Q_o = Q of the coil without the sample. This means that $\Delta R \geq R_o$, where R_o is the resistance of the coil. For good quality coils, Q_o is approximately independent of frequency. Applying the criterion that $\Delta R \geq R_o$ and assuming that Q_o is constant one obtains useful design formula for minimum and maximum frequency limits for a material of given conductivity. The cylindrical monocrystal is considered.

(i) Low frequency limit $br_o = (\omega\sigma\mu_o)^{\frac{1}{2}} r_o \leq \frac{1}{2}$,

where r_o = radius of the cylindrical sample.

The change in resistance of the solenoid is,

$$\frac{\Delta R}{\omega L_o} = K_c \frac{(b r_o)^2}{8}, \tag{A19}$$

where

$$K_c = \frac{r_o^2 l_o}{r_c^2 l_c}, \tag{A13}$$

and r_c = radius and l_c = length of solenoid.

Requiring that

$$\frac{\Delta R}{\omega L_o} \geq \frac{R_o}{\omega L_o} = \frac{1}{Q_o},$$

gives

$$1 \leq \frac{\Delta R}{R_o} = K_c Q_o \frac{(b r_o)^2}{8},$$

Facing Page 12

FIGURE 4

RANGE OF CONDUCTIVITIES MEASUREABLE WITH A COIL OF Q-FACTOR Q_o AS A FUNCTION OF FREQUENCY

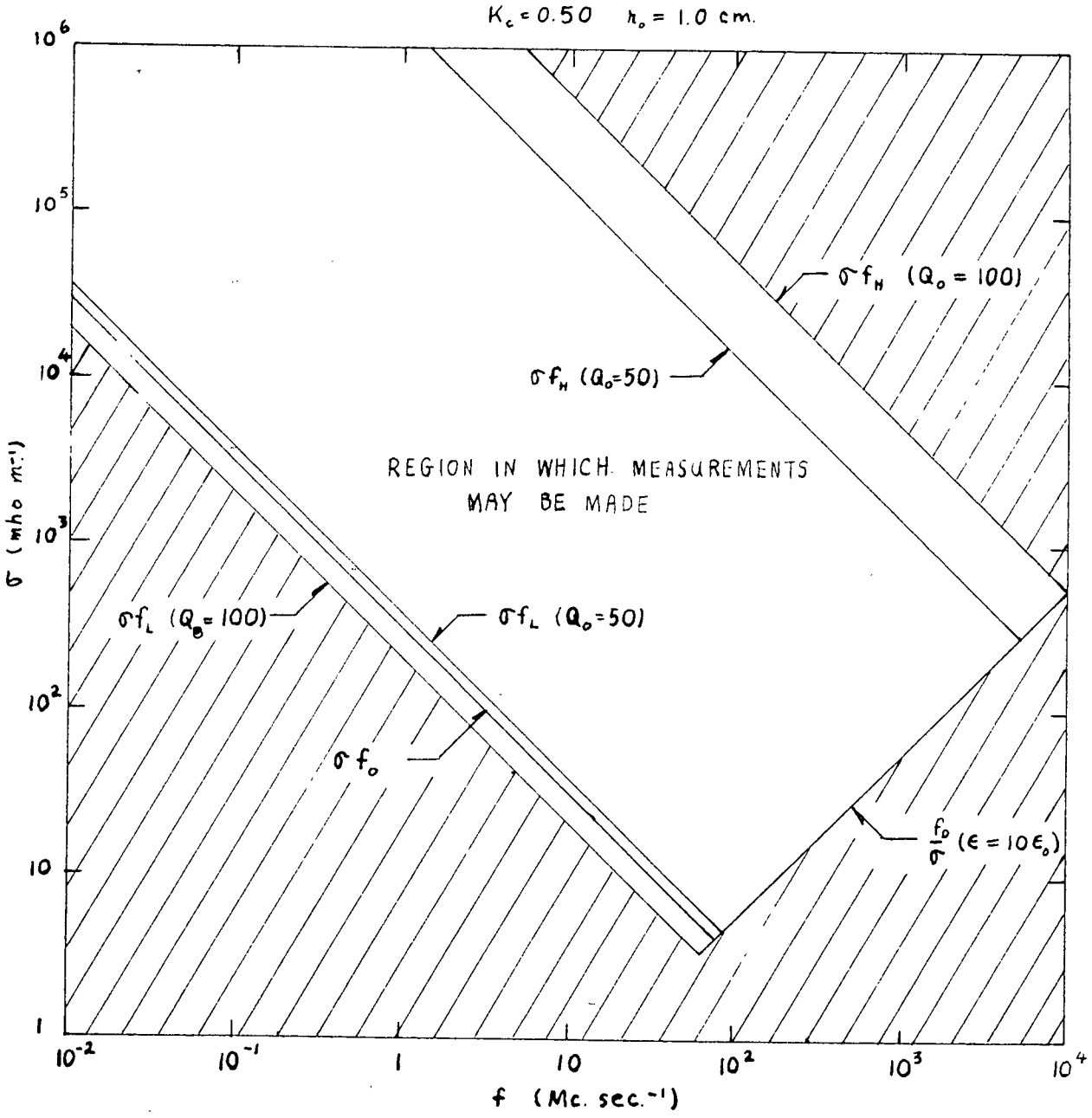

or $$f_L \sigma = \frac{8}{2\pi \mu_o r_o^2 K_c Q_o}, \tag{5}$$

where f_L = low frequency limit.

(ii) High frequency limit $br_o \geq 10$.

The change in resistance of the solenoid is,

$$\frac{\Delta R}{\omega L_o} = \frac{\sqrt{2}\, K_c}{b r_o} \tag{A22}$$

Requiring that $$\frac{\Delta R}{\omega L_o} \geq \frac{R_o}{\omega L_o} = \frac{1}{Q_o},$$

gives $$1 \leq \frac{\Delta R}{R_o} = \frac{\sqrt{2}\, K_c Q_o}{b r_o},$$

or $$f_H \sigma = \frac{K_c^2 Q_o^2}{\pi \mu_o r_o^2}, \tag{6}$$

where f_H = high frequency limit.

A second design criterion is that the Q of the coil should be as large as possible in order that the lower and upper frequency limits may be extended. Thus it would be possible to study a wider range of conductivities with the same coil. A high Q requires in general that L, the inductance of the coil, be large. The minimum value of the tuning capacitance, C_m, of the Q-meter limits the maximum value of the inductance to L_M, assuming that the frequency is fixed at f_o by other considerations. C_m is fixed by the requirement that the tuning capacitance be large compared to C_s, the stray capacitance of the coil, and to the combined capacitance of the connecting cable and the internal capacitance of the vacuum tube voltmeter measuring $\mathcal{E}$. The radius r_c and length l_c of the solenoid are also fixed by the size of the sample. Hence

$$L_M = \mu_o N_M^2 \frac{\pi r_c^2}{l_c} = \frac{1}{\omega_o^2 C_m}, \tag{7}$$

giving $$N_M = \frac{1}{2\pi r_c f_o} \left(\frac{l_c}{\mu_o \pi C_m} \right)^{\frac{1}{2}}. \tag{8}$$

as the maximum number of turns on the solenoid.

A limitation, applying in particular to low conductivity materials, is the requirement that the displacement currents be negligible. Now conduction currents are proportional to σ and displacement currents are proportional to $\omega\epsilon$. Hence if one requires that $\frac{\omega\epsilon}{\sigma} \leq 1/100$ say. Then

$$\frac{f_D}{\sigma} \leq \frac{1}{200\pi\epsilon_r\epsilon_o} = \frac{180}{\epsilon_r} \quad \text{Mc ohm m}, \tag{9}$$

where ϵ_r = relative dielectric constant of the sample and f_D = high frequency limit due to displacement currents. The results of this section are summarized in Fig. 4.

(d) Frequency Range. Maximum sensitivity will be acheived when the fractional change in resistance, $\Delta R/R$ is a maximum. The reason for this maximum is seen by considering the two competing factors. At low frequencies the exciting magnetic field is uniform throughout the material and the eddy currents increase linearly with radius and frequency. At higher frequencies, that is when the penetration depth $1/b = 1/(\omega\sigma\mu_o)$ becomes small compared to the physical dimension r_o of the sample, the exciting field is attenuated as it penetrates into the sample and hence the eddy currents are concentrated in the surface, again decreasing ΔR. The variation of $\Delta R/\omega L_o$ and $\Delta L/L_o$ with frequency are shown in Fig. 1 for the long monocrystalline cylindrical sample case.

The low frequency region appears to be the most desirable one from an experimental viewpoint since the eddy currents are distributed more uniformly than in the high frequency region. A disadvantage of the high frequency region is that the current is concentrated in the surface and

hence any surface irregularities, chemical layers and other inhomogeneities will effect the value of σ. A further purely experimental disadvantage of using the high frequency region is that ΔL must be measured in addition to ΔQ, thus increasing the sources of error. Considering the factors mentioned above it was decided that the best frequency to use would be the one which made $br_o = \frac{1}{2}$. Here ΔR is a maximum under the constraints that $\Delta L/L < 1\%$ and that the low frequency formula for ΔR be accurate to better than 1%. This frequency will be denoted by f_o, where

$$f_o = \frac{1}{8\pi\mu_o\sigma h_o^2} \qquad (10)$$

2.2 Crossed Magnetic Field Hall Mobility Measurements

(a) Theory. Consider a spherical sample excited by an alternating magnetic field B_{z0}. Circulating eddy currents J_ϕ are then set up in the sample in the x-y plane, as shown in Fig. 5a. A static magnetic field B_x is now applied. The force on the current carriers is,

$$\vec{F} = q(\vec{v} \times \vec{B}_x).$$

and the current density in the x-y plane is,

$$\vec{J}_\phi = nq\vec{v},$$

where n = density of current carriers. Hence

$$\vec{J}_\phi \times \vec{B}_x = n\vec{F}$$

$$= nq\vec{E}_{eff.}$$

The component of current along the z-axis is,

$$\vec{J}_z = nq u_H \vec{E}_{eff.}$$

$$= u_H \vec{J}_\phi \times \vec{B}_x$$

$$= u_H B_x J_\phi \cos\phi \, \vec{z}_o, \qquad (11)$$

where $\vec{z}_o$ is a unit vector. Note that J_z is a maximum where it crosses the x-axis and zero where it crosses the y-axis. Hence the eddy current planes are in effect turned through an angle tan $u_H B_x$. The difference between the internal and external magnetic fields, $B_{zi} - B_{zo}$ will also be rotated through the Hall angle tan $u_H B_x$. The result is a component of magnetic field, B_Y, along the y-axis, where $B_Y = u_H B_x (B_{zi} - B_{zo})$. This

Facing Page 16

FIGURE 5

HALL MOBILITY MEASUREMENTS

(a) FIELD AND CURRENT RELATIONS

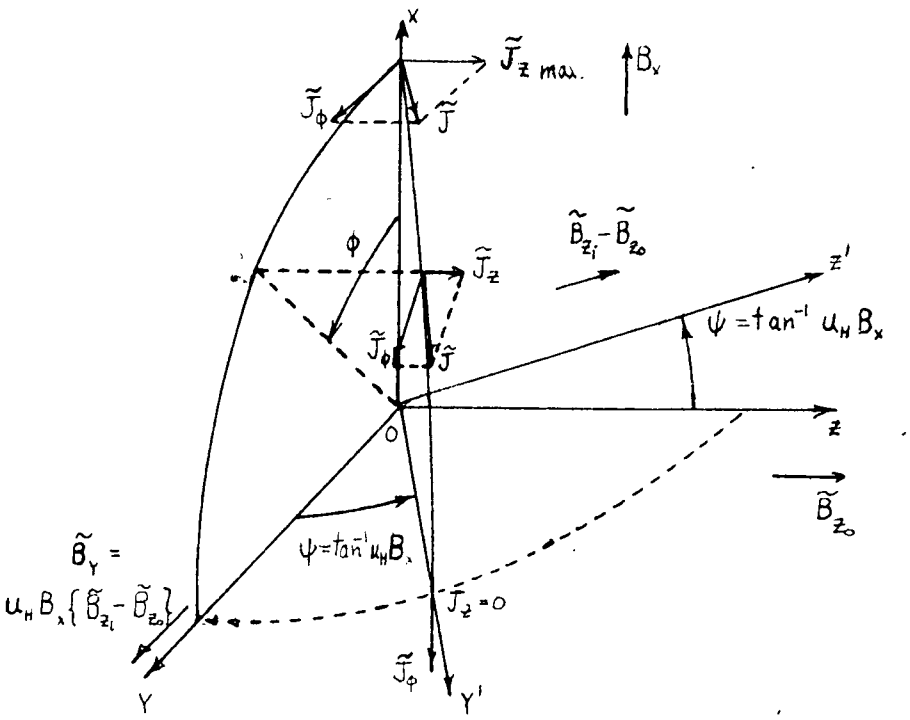

(b) CIRCUIT DIAGRAM

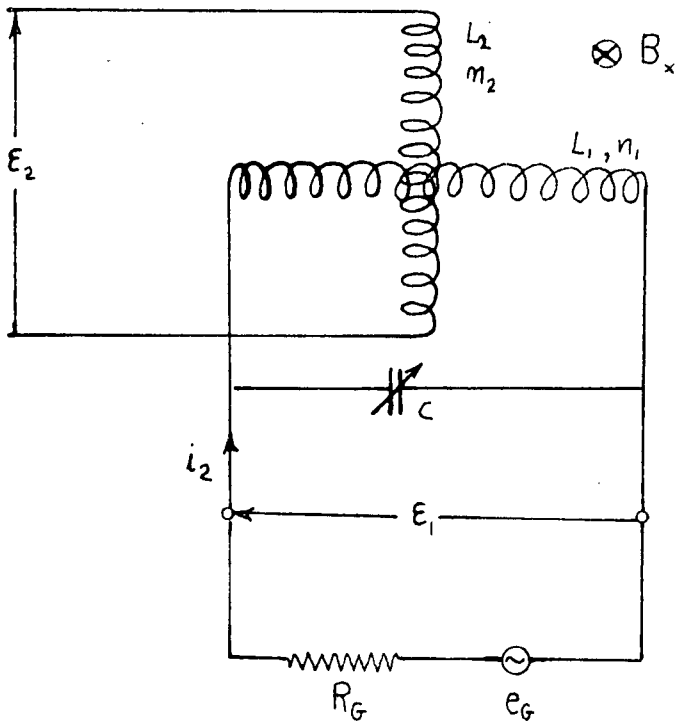

field is detected by a coil placed along the y-axis and the Hall mobility thus obtained.

A rigorous derivation for $\vec{J}$ in the general case is given in appendix E, part 3 using the conductivity tensor derived in appendix D. The conductivity tensor was derived under the assumptions of a velocity independent relaxation time, τ, and that 1/m is a scalar. Refer to Fig. 5b. The resistance reflected into coil 2 when the sample is excited by coil 1 is calculated in the low frequency limit $br_o = (\omega\sigma\mu_o)^{\frac{1}{2}} r_o \leq \frac{1}{2}$, for two special cases:

(i) A cylinder of radius r_o and length l_o, where $l_o >> r_o$ gives

$$R_{21} = \frac{\omega(b r_o)^2}{16}(\mu_o n_1 n_2 \pi r_o^2 l_o)\frac{u_H B_x}{1+(u_H B_x)^2}, \qquad \text{(E29)}$$

and (ii) a sphere of radius r_o gives

$$R_{21} = \frac{\omega(b r_o)^2}{20}(\mu_o n_1 n_2 \frac{4}{3}\pi r_o^3)\frac{u_H B_x}{1+(u_H B_x)^2}, \qquad \text{(E30)}$$

where n_1 = number of turns/m on coil 1 and n_2 = number of turns/m on coil 2.

With reference to Fig. 5b, $R_{21} = \mathcal{E}_2/i_1$, if $i_2 = 0$. Also

$$i_1 = \frac{\mathcal{E}_1}{R_1 + j\omega L_1},$$

and if $Q_1 >> 1$, then

$$i_1 \approx \frac{\mathcal{E}_1}{j\omega L_1}. \qquad (13)$$

Hence

$$R_{21} = \frac{\mathcal{E}_2}{\mathcal{E}_1}\omega L_1 \qquad (14)$$

and for the two cases:

(i) A cylinder gives

$$\frac{\mathcal{E}_2}{\mathcal{E}_1} = \frac{(b r_0)^2}{16} \cdot \frac{\mu_0 m_1 m_2 \pi r_0^2 l_0}{L_1} \cdot \frac{u_H B_x}{1 + (u_H B_x)^2}, \tag{15}$$

and (ii) a sphere gives

$$\frac{\mathcal{E}_2}{\mathcal{E}_1} = \frac{(b r_0)^2}{20} \cdot \frac{\mu_0 m_1 m_2 \frac{4}{3}\pi r_0^3}{L_1} \cdot \frac{u_H B_x}{1 + (u_H B_x)^2}. \tag{16}$$

A further extension of the theory makes it possible to make measurements independent of the parameter b and independently of the size and the shape of the sample at low frequencies. Hence the conductivity need not be known. In particular, if R_{11} is the resistance change reflected into the exciting coil, as given by (E22) and (E23), then

$$R_{21} = R_{11} \cdot \frac{m_2}{m_1} \cdot \frac{(u_H B_x)/2}{1 + (u_H B_x)^2/2}, \tag{17}$$

using (E29) and (E30). Thus on combining (13) and (17),

$$\frac{\mathcal{E}_2}{\mathcal{E}_1} = \frac{R_{11}}{\omega L_1} \cdot \frac{m_2}{m_1} \cdot \frac{(u_H B_x)/2}{1 + (u_H B_x)^2/2}. \tag{18}$$

Now
$$R_{11} = \omega L_1 \left(\frac{1}{Q_{s1}} - \frac{1}{Q_{o1}} \right), \tag{1}$$

where Q_{s1} is the Q of coil 1 with the sample and Q_{o1} without the sample.

Finally,
$$\frac{\mathcal{E}_2}{\mathcal{E}_1} = \left(\frac{1}{Q_{s1}} - \frac{1}{Q_{o1}} \right) \cdot \frac{m_2}{m_1} \cdot \frac{(u_H B_x)/2}{1 + (u_H B_x)^2/2}. \tag{19}$$

If R_{22}, the resistance reflected into coil 2 when used as the exciting coil, is measured, rather than R_{11}, then

$$R_{21} = R_{22} \cdot \frac{m_1}{m_2} \cdot \frac{(u_H B_x)/2}{1 + (u_H B_x)^2/2}, \tag{20}$$

giving
$$\frac{\mathcal{E}_2}{\mathcal{E}_1} = \frac{R_{22}}{\omega L_1} \cdot \frac{m_1}{m_2} \cdot \frac{(u_H B_x)/2}{1 + (u_H B_x)^2/2}. \tag{21}$$

Now $$\Delta R_{22} = \omega L_2 \left(\frac{1}{Q_{S2}} - \frac{1}{Q_{o2}} \right), \tag{1}$$

where Q_{S2} is the Q of coil 2 with the sample and Q_{o2} without the sample.

Finally, $$\frac{\mathcal{E}_2}{\mathcal{E}_1} = \left(\frac{1}{Q_{S2}} - \frac{1}{Q_{o2}} \right) \cdot \frac{n_1 L_2}{n_2 L_1} \cdot \frac{(u_H B_x)/2}{1 + (u_H B_x)^2/2} . \tag{22}$$

(b) Design Considerations. Consider the design of an experiment to measure the Hall mobility, u_H, of a cylindrical sample in the low field region where $(u_H B)^2 << 1$. In particular, the most useful formula for experimental work is,

$$\frac{\mathcal{E}_2}{\mathcal{E}_1} = \left(\frac{1}{Q_{S2}} - \frac{1}{Q_{o2}} \right) \cdot \frac{n_1 L_2}{n_2 L_1} \cdot \frac{(u_H B_x)/2}{1 + (u_H B_x)^2/2} , \tag{22}$$

where coil 1 is the exciting coil and coil 2 is the pickup coil.

One requires that the pickup voltage, $\mathcal{E}_2$, be a maximum in order to obtain greatest sensitivity. This requires that B_x, L_2/n_2, $\mathcal{E}_1 n_1/L_1$ and $1/Q_{S2} - 1/Q_{o2}$ be a maximum. The physical size of the sample will be assumed to be fixed at radius r_o and length l_o by other considerations. The following limits to the parameters can then be set:

(i) $br_o = \frac{1}{2}$ is the largest value at which the low frequency approximation is accurate to better than 1%. Thus at

$$f_o = \frac{1}{8\pi\sigma\mu_o r_o^2}, \tag{10}$$

$$\frac{\Delta R}{\omega L_2} = \left(\frac{1}{Q_{S2}} - \frac{1}{Q_{o2}} \right) \tag{1}$$

is a maximum.

(ii) B_x is limited to approximately 0.6 W m^{-2} by the design of the magnet and by the size of the sample.

(iii) $L_2/n_2 \propto n_2 V_{C2}$, where V_{C2} = volume of coil 2, is limited by the

shunt capacitance C_2 of coil 2. If coil 2 resonates at frequency f_2 due to C_2, then one would require that $f_2 \geq 10 f_o$ say. Now C_2 includes the internal capacitance of the vacuum tube voltmeter and of the connecting cable and will be of the order of 50 to 100 pf. Hence if the minimum volume of coil 2 which will hold the sample is V_{c2} then,

$$L_2 = \mu_o n_2^2 V_{c2} = \frac{1}{\omega_2^2 C_2} = \frac{1}{100\,\omega_o^2 C_2}.$$

But
$$f_o = \frac{1}{8\pi\sigma\mu_o h_o^2}, \tag{10}$$

giving
$$n_{2\,max.} = \frac{2\sigma h_o^2}{5}\left(\frac{\mu_o}{C_2 V_{c2}}\right)^{\frac{1}{2}}, \tag{23}$$

as the maximum number of turns/m.

(iv) The maximization of $\mathcal{E}_1 n_1/L_1 \propto \mathcal{E}_1/\sqrt{L_1}$. Consider the circuit in Fig. 2a. At resonance, $Z = Q_1 \omega L_1$.

Hence
$$\frac{\mathcal{E}_1}{e_g} = \frac{\omega L_1 Q_1}{R_G + \omega L_1 Q_1},$$

giving
$$\frac{\mathcal{E}_1 n_1}{L_1} \propto \frac{\omega \sqrt{L_1}\, Q_1}{R_G + \omega L_1 Q_1},$$

which is maximized when

$$L_{1\,opt.} = \frac{R_G}{\omega Q_1}, \tag{24}$$

corresponding to an impedance match of the generator to the turned inductor.

Note that n_1 is defined as the equivalent number of turns/m on a solenoid producing the same field. In particular, for a solenoid

$$B_1 = \mu_o n_1 i_1,$$

while for a Helmholtz pair, the field at the center is,

$$B_1 = \mu_o i_1 \left\{ \frac{4N}{\pi} \frac{l^2}{(l^2+a^2)\sqrt{2l^2+a^2}} \right\}, \tag{25}$$

where 2l = length of side of square coil,

2a = separation of the two coils,

N = turns per coil,

and i_1 = current per coil

Hence $$n_1 = \frac{4N}{\pi} \cdot \frac{l^2}{(l^2+a^2)\sqrt{2l^2+a^2}}. \tag{26}$$

Now n_1 will be constant only in a region near the center of the Helmholtz pair and hence the sample should be small enough so that it is contained in this region.

Large error signals will be detected if the exciting and pickup coils are not precisely perpendicular. Hence it is particularly important that the coils be adjustable in order to achieve this condition. In particular, if the coils are out of perpendicular by an angle θ, then the error signal will be,

$$\begin{aligned} \mathcal{E}_e &= \omega B_{z1} A N_2 \sin\theta \\ &= \omega B_{z1} n_2 V_{c2} \sin\theta \\ &= i_1 \omega (\mu_o n_1 n_2 V_{c2}) \sin\theta, \end{aligned} \tag{27}$$

where V_{c2} = volume of coil 2.

Now $\mathcal{E}_2 = i_1 \Delta R_{21}$

$$= i_1 \omega \frac{(b r_o)^2}{16} (u_H B_x)(\mu_o n_1 n_2 \pi l_o r_o^2), \tag{E29}$$

for a cylinder at low frequencies, ($br_o \leq \frac{1}{2}$), and for low fields such that $(u_H B_x)^2 << 1$. Thus,

$$\frac{\mathcal{E}_e}{\mathcal{E}_2} = \frac{V_{c2}\, 16 \sin\theta}{V_S\, u_H B_x (b r_o)^2} \quad (28)$$

where the volume of the sample, $V_S = \pi r_o^2 l_o$.

If say $V_{c2} = 2V_S$ and $(br_o)^2 = \frac{1}{2}$, then

$$\frac{\mathcal{E}_e}{\mathcal{E}_2} = \frac{64 \sin\theta}{u_H B_x}.$$

Now for small angles $\sin\theta \simeq \theta$ rad $= \theta^\circ/57.3$.

Hence

$$\frac{\mathcal{E}_e}{\mathcal{E}_2} = \frac{1.1\,\theta^\circ}{u_H B_x} \quad (29)$$

Consider a typical material with $u_H = 0.10$ m^2 V^{-1} sec^{-1} and $B_x = 0.5$ W m^{-2}. It is seen that an angle of $\theta = \frac{1}{2}^\circ$ results in an error signal $\mathcal{E}_e = 11\mathcal{E}_2$ and that the seriousness of this type of error increases with materials of decreasing mobility.

A source of error can be resistance and inductance changes reflected into the coils from the poles and frame of the electromagnet. If the Helmholtz coils, solenoid and sample are centered accurately between the magnet poles the resistance changes reflected into the coils by the induced eddy currents will cancel by symmetry. It should be noted that these changes can be a function of B because of the variable permeability of the steel pole pieces. In particular, a 1% change in resonant frequency of the Helmholtz pair was noted when the field was increased from 0 to 0.5 W m^{-2}.

Another source of error is electrostatic coupling. The pickup coil may be electrostatically shielded by enclosing it in a grid of orthogonal non-intersecting wires. They are connected to a common ground only at one point so that eddy currents are not set up around the grid.

(c) Description of Apparatus. The static magnetic fields were produced by a Newport Instruments Type A Electromagnet. The electromagnet was controlled by a Varian Associates Model V2300A Power Supply and Model V2301A Current Regulator. The mild steel pole pieces were 10 cm in diameter and the spacing was continuously adjustable from 0 to 11.0 cm. The maximum continuous allowable current per winding for the electromagnet was 4 amp. These windings were connected in series since the maximum current available from the power supply and regulator was also 4 amp. Some useful maximum field and homogeneity data is given below.

Air gap (cm)	Field strength at maximum rated current of 4 amp per coil (W m^{-2})	Approximate radial distance from center at which field falls off by 1% from central value (cm)	Approximate radial distance from center at which field falls off by 10% from central value (cm)
10	---	1.3	3.5
5	0.56	2.4	4.1
3	0.77	---	---
2.5	0.87	3.6	4.6
2	0.97	---	---

The static magnetic fields were measured using a Radio Frequency Laboratories, Model 1295 Gaussmeter. Its range is 0.01 to 2 W m^{-2} in 9 ranges and it has standard magnets for calibration.

A pair of Helmholtz coils were built around the pole pieces and a solenoid was mounted on the frame of the Helmholtz coils, centrally between the coils and the magnet pole faces. In particular, the Helmholtz pair were rigidly mounted on a wooden frame, the geometry of which ensured orthogonality with respect to the static magnetic field. The solenoid

was suspended from the top Helmholtz coil by 2 adjustable brass bolts. The axis of the solenoid was perpendicular to the axes formed by the lines joining the centers of the magnet poles and the centers of the Helmholtz coils. The adjustable bolts enabled one to obtain a null signal on the pickup coil with the static field zero. Brass rather than steel fasteners were used throughout to minimize field distortions.

The Shasta sine wave generator and the 2 Hewlett-Packard vacuum tube voltmeters mentioned in 2.1b were used. Two 2 ft lengths of RG58A-U coaxial cable joined the Helmholtz pair, connected in parallel, to a vacuum tube voltmeter and the sine wave generator. A condensor box was connected across the generator and the circuit was tuned for parallel resonance to acheive maximum power input into the coils as indicated by a maximum in $\mathcal{E}_1$, the voltage across the coils. The coupling between the Helmholtz pair was negligible.

A third 2 ft length of RG58A-U connected the pickup coil to the second vacuum tube voltmeter. The Helmholtz pair, the solenoid and the coaxial leads were connected to a common ground near the solenoid. Shielded leads were used wherever possible to minimize stray pickup, such as 60 cps.

2.3 Electrodeless Magnetoresistance Measurements

When the product $u_H B$ becomes comparable with or greater than unity, the phenomena of magnetoresistance is pronounced. Two special cases will be considered.

(a) Transverse Magnetoresistance. The exciting and static magnetic fields, $\tilde{B}_{z0}$ and B_z, are parallel, resulting in the static field being perpendicular to the eddy current planes. B_z will exert a radial force on the current causing it to concentrate in the outer or inner layers of the sample, depending on the signs of $\tilde{B}_{z0}$ and B_z. Hence if the resistance reflected into the solenoid by the sample is measured it will decrease with increasing B_z. In particular, two cases have been calculated for the low frequency region, $br_o \leq \frac{1}{2}$, assuming constant τ and that $1/m$ is a scalar:

(i) A cylinder of length l_o and radius r_o gives,

$$\frac{\Delta R}{\omega L_o} = K_c \frac{(br_o)^2}{8} \cdot \frac{1}{1+(u_H B_z)^2}, \qquad \text{(E11)}$$

where

$$K_c = \frac{r_o^2 l_o}{r_c^2 l_c}. \qquad \text{(E13)}$$

and (ii) a sphere of radius r_o gives,

$$\frac{\Delta R}{\omega L_o} = K_s \frac{(br_o)^2}{10} \frac{1}{1+(u_H B_z)^2}, \qquad \text{(E14)}$$

where

$$K_s = \frac{4 r_o^3}{3 r_c^2 l_c}. \qquad \text{(E16)}$$

The design criteria for a suitable coil and a Q-meter to measure $\Delta R(B_z)$, are the same as in 2.1. However certain precautions must be taken because of the following difficulties. First of all, it is

possible that eddy currents will be induced in the magnet pole pieces and hence reflect a resistance into the coil. This effect would also be a function of B_z since the permeability of the steel is a function of B_z, and it is best eliminated by measuring the Q of the coil as a function of B_z both with and without the sample. The solenoid is set up in a suitable non-metallic stand with axis along the line joining the center of the two magnet poles.

(b) Mixed Magnetoresistance. The exciting and static magnetic fields, $\tilde{B}_{z0}$ and B_x, are perpendicular, resulting in the static field being parallel to the plane of the eddy current. Hence B_x will cause a rotation of the eddy current planes as explained in 2.2. The x-component of the eddy currents will be unaffected, whereas the y-component of the eddy currents is decreased and a z-component appears. These results are derived in appendix E, part 3. The z-component has no effect on the exciting solenoid since there is no effective E_z. Hence if the resistance reflected into the solenoid is measured it will decrease with increasing B_x. In particular, two cases have been calculated for the low frequency limit, $br_o \ll \frac{1}{2}$, assuming constant τ and that 1/m is a scalar:

(i) A cylinder of length l_o and radius r_o gives

$$\frac{\Delta R}{\omega L_o} = K_c \frac{(br_o)^2}{8} \frac{1 + (u_H B_x)^2/2}{1 + (u_H B_x)^2}, \tag{E22}$$

where

$$K_c = \frac{r_o^2 l_o}{r_c^2 l_c}. \tag{E13}$$

and (ii) a sphere of radius r_o gives

$$\frac{\Delta R}{\omega L_o} = K_s \frac{(br_o)^2}{10} \frac{1 + (u_H B_x)^2/2}{1 + (u_H B_x)^2}, \tag{E23}$$

where

$$K_s = \frac{4 r_o^3}{3 r_c^2 l_c}. \tag{E16}$$

The remarks concerning experimental difficulties in (a) apply again here. However, the effect of the eddy currents induced in the pole pieces will be much smaller since the solenoid axis is orthogonal to the line joining the centers of the pole pieces. If the solenoid is set up symmetrically between the pole pieces these effects should cancel.

CHAPTER 3 - EXPERIMENTAL RESULTS

3.1 Conductivity Measurements on Graphite

Conductivity measurements were made on commercial graphite by the eddy current technique of 2.1 and by a 4-electrode technique. Thus it was possible to check the accuracy of the electrodeless technique. Graphite was chosen because it was easily obtained in the form of a long solid homogeneous cylinder and secondly because its conductivity is of the same order of magnitude as that of the silver selenide salt discussed in part II. The sample of radius r_o = 1.0 cm and length l_o = 6.1 cm was prepared from the cylindrical core of a 6-volt dry cell.

(a) Electrodeless Technique. The conductivity is given by (1) and (A19) in the low frequency limit $br_o \leq \frac{1}{2}$, as

$$\sigma = \frac{K_1}{f}\left(\frac{1}{Q_1} - \frac{1}{Q_o}\right), \tag{30}$$

where

$$K_1 = \frac{4}{\pi \mu_o r_o^2 K_c}, \tag{31}$$

and

$$K_c = \frac{r_o^2 l_o}{r_c^2 l_c}. \tag{A13}$$

The radius of the solenoid r_c = 1.3 cm and the length of the solenoid l_c = 10.3 cm. Hence $K_1 = 2.9\times10^{10}$ mho m^{-1} sec^{-1}. The Q-meter described in 2.1 and Fig. 2b and 3 was used to measure the Q's.

Experimental results:

f (kc)	$1/Q_o$	$1/Q_1$	σ (mho m^{-1})	br_o
22.7	5.11×10^{-2}	6.58×10^{-2}	1.9×10^{4}	0.23
128	3.11×10^{-2}	12.02×10^{-2}	2.0×10^{4}	0.56
197	0.15×10^{-2}	13.35×10^{-2}	1.75×10^{4}	0.66

(b) 4-Electrode Technique. The standard method in which the current electrodes are attached to the ends of the sample and two potential probes are placed along the sample was used. This method eliminates the errors due to contact resistance and rectifying contacts inherent in a 2-electrode method. The ends and two narrow bands on the sample were painted with silver paint in order to obtain good contact with the electrodes. Now

$$\frac{\mathcal{E}}{I} = R = \frac{l_1}{\pi r_o^2 \sigma} \quad . \tag{32}$$

where r_o = 1.0 cm, and the distance between the potential probes l_1 = 5.2 cm. Hence

$$\sigma = 1.66 \times 10^2 \frac{I}{\mathcal{E}} \text{ mho m}^{-1}$$

Experimental results:

f (kc)	$\mathcal{E}$ (mv)	I (amp)	σ (mho m^{-1})
0	6.90	1.00	2.4×10^4
0.1	20.2	3.27	2.7×10^4
1	23.3	3.60	2.6×10^4
10	10.0	1.57	2.6×10^4
20	6.85	1.00	2.4×10^4

The discrepancy of 24% between the average results obtained from the two methods is considered satisfactory because of errors inherent in the electrodeless method. In particular,

(i) Fringing of the exciting field, due to the long solenoid approximation not being satisfied, results in too low a value of observed σ, and (ii) Disruption of the eddy current patterns at the ends of the sample, an error which would decrease as the length to radius ratio of the cylinder was increased, would also result in too low a value of observed σ.

3.2 Electronic Properties of N-Type Germanium

Conductivity and Hall mobility measurements were made on a single crystal of n-type germanium to illustrate the techniques described in 2.1 and 2.2. The crystal, while somewhat irregular in shape, was assumed to be spherical for purposes of calculation. In addition, the crystal was purer at one end than the other and hence contained impurity concentration gradients. Thus the conductivity and mobility would be a function of position. However these effects are not calculable and it was assumed that the theory gave average values for the conductivity and mobility. All measurements are made in the low frequency region $br_o = (\omega\sigma\mu_o)^{\frac{1}{2}} r_o \leq \frac{1}{2}$, where r_o is the radius of the sphere.

(a) Conductivity Measurements. The conductivity is given by

$$\sigma = \frac{K_1}{f}\left(\frac{1}{Q_1} - \frac{1}{Q_o}\right), \tag{30}$$

where

$$K_1 = \frac{10}{2\pi\mu_o r_o^2 K_s}, \tag{33}$$

and

$$K_s = \frac{4 r_o^3}{3 r_c^2 l_c}. \tag{B8}$$

The Q-meter described in 2.1b and Fig. 2b and 3 was used to measure the Q's of the coil.

Experimental data: $r_o = 1.2$ cm and $K_s = 0.47$, giving $K_1 = 1.9\times10^{10}$ mho m^{-1} sec^{-1}, and

$$\sigma = \frac{1.9\times10^{10}}{f}\left(\frac{1}{Q_1} - \frac{1}{Q_o}\right) \text{ mho } m^{-1}.$$

The Q-meter readings at f = 690 kc are $1/Q_1 = 0.126$ and $1/Q_o = 0.0124$. Hence $\underline{\sigma = 3.1\times10^{3} \text{ mho } m^{-1}}$.

(b) Hall Mobility Measurements. The Hall mobility is given by

$$u_H = \frac{2V_2}{V_1 B_x} \cdot \frac{n_2 L_1}{n_1 L_2} \cdot \frac{Q_{o2} Q_{s2}}{Q_{o2} - Q_{s2}}, \qquad (22)$$

for $(u_H B_x)^2 << 1$, the quantities being defined in detail in 2.2a and Fig. 5b. The apparatus and procedure was as described in 2.2c.

Experimental data:

$L_1 = 7.5\,\mu h$	$n_1 = 40$ turns m^{-1}
$L_2 = 15\,\mu h$	$n_2 = 7.7 \times 10^2$ turns m^{-1}
$f = 500$ kc	$B_x = 0.10$ W m^{-2}
$V_1 = 10.3$ v	$V_2 = 0.51$ mv
$Q_{o2} = 111$	$Q_{s2} = 10.9$

Substituting the above data in (22), one obtains $u_H = 0.12\ m^2\ v^{-1}\ sec^{-1}$. Also of interest is the donor density

$$N_D \simeq \frac{\sigma}{u_H e} = 1.6 \times 10^{23}\ m^{-3}.$$

The experimentally determined value for u_H may be compared with the value given by Prince (1953). In particular, for $N_D = 10^{23}\ m^{-3}$, he quotes $u_m \simeq 0.20\ m^2\ v^{-1}\ sec^{-1}$ and $u_H/u_m \simeq 0.9$, giving $u_H \simeq 0.18\ m^2\ v^{-1}\ sec^{-1}$. The agreement between the results is satisfactory because of the large errors possible due to the irregular shape of the sample and the non-uniformity of N_D through the sample. These errors are most serious in determining the conductivity and hence indirectly in obtaining N_D.

3.3 Electronic Properties of N-Type Indium Antimonide

Conductivity, magnetoresistance and Hall mobility measurements were made on a single crystal of n-type indium antimonide using the electrodeless techniques of 2.1, 2.2 and 2.3 and by dc 4-electrode techniques. The exceptionally high electron mobility of indium antimonide made it possible to acheive experimentally, values of $u_H B > 1$, and thus the phenomena of magnetoresistance was pronounced. The sample was irregular in shape and was approximated by a cylinder for purposes of calculation.

(a) Conductivity Measurements.

(i) Electrodeless Technique. The method and apparatus are described fully in 2.1. In particular the conductivity

$$\sigma = \frac{K_1}{f}\left(\frac{1}{Q_1} - \frac{1}{Q_0}\right), \tag{30}$$

where

$$K_1 = \frac{10^7 r_c^2 l_c}{\pi^2 r_0^4 l_0}. \tag{31}$$

Now r_c = 1.6 cm, l_c = 3.0 cm, r_0 = 0.50 cm and l_0 = 2.7 cm, giving $K_1 = 4.6\times10^{11}$ mho m^{-1} sec^{-1}. The Q-meter readings at f = 264 kc are Q_1 = 27.9 and Q_0 = 39.6. Hence $\underline{\sigma = 1.8\times10^4 \text{ mho } m^{-1}}$, and br_0 = 0.96.

(ii) DC 4-Electrode Technique. The same technique as described in 3.1b was used. Hence

$$\sigma = \frac{l_1 I}{A \mathcal{E}},$$

where A ≃ 1.0 cm^2 and the distance between the potential probes l_1 = 1.7 cm.

Thus

$$\sigma = 1.7 \times 10^2 \frac{I}{\mathcal{E}} \text{ mho } m^{-1}.$$

Experimental results gave $\mathcal{E}$ = 7.8 mv for I = 1.0 amp, giving $\underline{\sigma = 2.2\times10^4 \text{ mho } m^{-1}}$.

Facing Page 32

FIGURE 6

TRANSVERSE MAGNETORESISTANCE CURVES

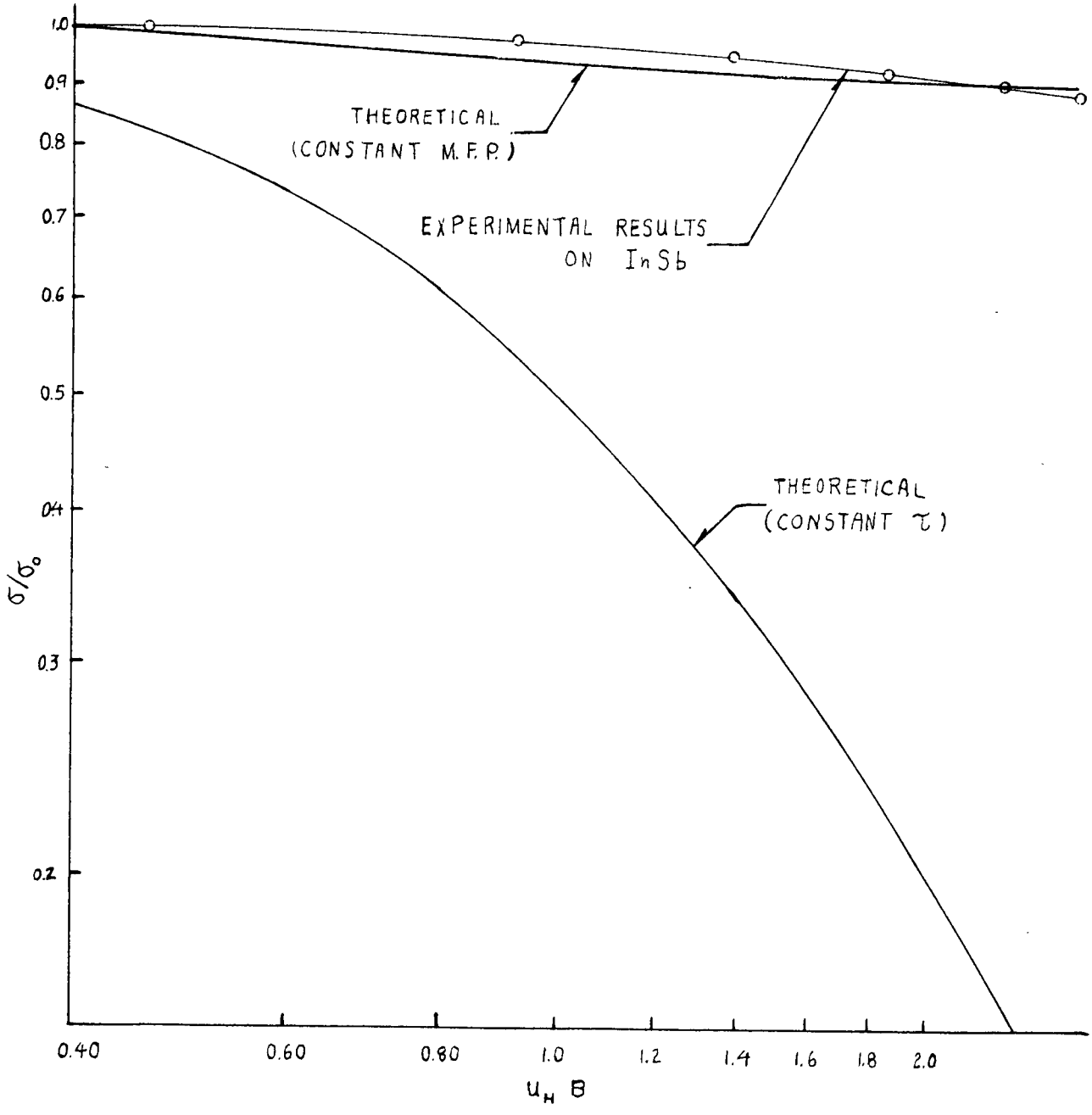

(iii) Discussion of Results. The agreement between the results is satisfactory because of the errors inherent in the electrodeless method, as mentioned in 3.1, and because of the irregular shape of the sample. In particular, r_o, the radius of the cylinder, can only be estimated to $\pm$ 25%. Another error is due to making the measurements at a frequency such that $br_o \simeq 1$, resulting in an error of 4% in the low frequency formula.

(b) Magnetoresistance Measurements. Two magnetoresistance experiments are made.

(i) Transverse Magnetoresistance. The static magnetic field B_z, is perpendicular to the plane of the eddy currents. The procedure and apparatus were described in 2.1 and 2.3. In particular, one measures experimentally

$$\frac{\Delta R(B_z)}{\omega L_o} = \frac{1}{Q_1} - \frac{1}{Q_o} \quad . \tag{1}$$

whereas theoretically, $\frac{\Delta R}{\omega L_o} = \frac{a}{1 + (u_H B_z)^2}$.

where $a = \frac{(br_o)^2}{8} \cdot \frac{r_o^2 l_o}{r_c^2 l_c}$.

In Fig. 6, the experimental data $1/Q_1 - 1/Q_o$ is plotted against B_z, and $\frac{a}{1 + (u_H B_z)^2}$ is plotted against $u_H B_z$. It is seen that the experimental results do not fit the theoretical curve which was derived on the basis of a constant mean free time, τ, between collisions.

The Lorentz-Sommerfeld theory of conduction based on the assumption of a constant mean free path will be considered for comparison. Wilson (1954) gives a curve for σ versus $u_H B$ for the transverse magnetoresistance effect. The assumptions are free electrons in one energy band, acoustic lattice scattering, constant mean free path and classical statistics.

Facing Page 33

FIGURE 7

MIXED MAGNETORESISTANCE CURVES

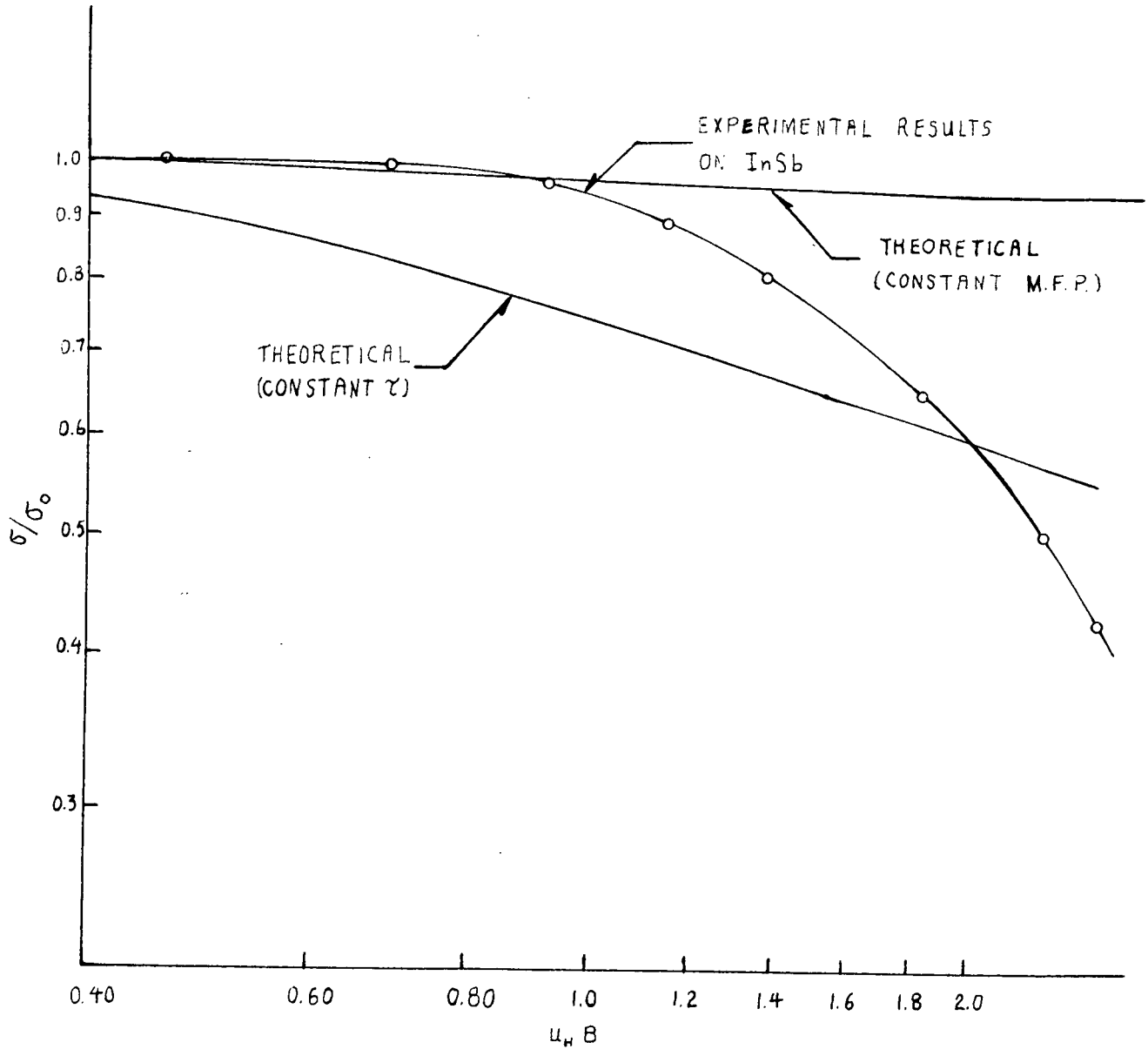

These results are plotted in Fig. 6 for comparison with the experimental results and with the constant τ theory. The theory is extended to a two band model for indium antimonide by Fischer and MacDonald (1958), but the results are not required here since the sample is n-type and hence the conductivity is predominantly due to electrons since $u_n \gg u_p$.

(ii) Mixed Magnetoresistance. The static field B_x, is parallel to the plane of the eddy currents, hence the resistance is a mixture of one-half transverse magnetoresistance and one-half longitudinal magnetoresistance as shown in appendix E, part 2. The procedure and apparatus were described in 2.1 and 2.3. In particular, one measures experimentally

$$\frac{\Delta R(B_x)}{\omega L_o} = \left(\frac{1}{Q_1} - \frac{1}{Q_o} \right), \tag{1}$$

as in (i), while theoretically

$$\frac{\Delta R}{\omega L_o} = a \, \frac{1 + (u_H B_x)^2/2}{1 + (u_H B_x)^2}, \tag{E22}$$

where $$a = \frac{(b r_o)^2}{8} \cdot \frac{r_o^2 l_o}{r_c^2 l_c}.$$

In Fig. 7, the experimental data, $1/Q_1 - 1/Q_o$ is plotted against B_x, and $a\frac{1+(u_H B_x)^2/2}{1+(u_H B_x)^2}$ is plotted against $u_H B_x$. It is noted that the theoretical $\Delta R(B_x)$ saturates at $\Delta R(0)/2$ while the experimental values appear to keep on decreasing.

The constant mean free path theory will also be considered for comparison with the experimental results. Now the total resistance measured will have equal contributions from the longitudinal and transverse components. Hence the curve given by Wilson (1954) for the transverse effect may be used. Glicksman (1957) states that there is no Hall effect and no magnetoresistance in the longitudinal case as long as m^* and τ are isotropic.

The curve showing the combination of these two results is plotted in Fig. 7.

(iii) Discussion of Results. The experimental transverse magnetoresistance results agree very well with the theoretical constant mean free path curve indicating that the mean free path hypothesis is satisfied. Note that theoretically as $u_H B \to \infty$, $\sigma/\sigma_o \to 0.868$ for spherical energy surfaces and constant mean free path.

The experimental mixed magnetoresistance results agree with the constant mean free path curve theory at values of $u_H B < 1$. The constant mean free path curve saturates at a value of $\sigma/\sigma_o = 0.934$ assuming spherical energy surfaces. However, for $u_H B > 1$ the experimental curve decreases rapidly and falls below the constant τ curve which saturates at $\sigma/\sigma_o = 0.50$.

Glicksman (1957) comments on the magnetoresistance at strong magnetic fields. In the limit of infinite fields, the magnetoresistance is expected to saturate, the saturation value depending on the form of the relaxation time and the energy surfaces. The saturation longitudinal magnetoresistance is independent of the energy dependence of τ and can directly provide information on K, the isotropy factor. For spherical energy surfaces K = 1, and the longitudinal magnetoresistance is zero. The saturation transverse magnetoresistance, σ/σ_o, may be much larger than $9\pi/32$ ($\tau \propto \text{energy}^{-\frac{1}{2}}$) for spherical energy surfaces and does depend on the energy dependence of τ. For example, if $\tau \propto (\text{energy})^{\frac{3}{2}}$, the value of $9\pi/32$ becomes $9\pi/96$. It is also noted that the saturation values of magnetoresistance are independent of the Hall mobility.

Dresselhaus, Kip, Kittel and Wagoner (1955) have observed cyclotron resonance in a single crystal of indium antimonide at a frequency of about 24,000 Mc. One resonance line observed at low field strengths corresponded to an effective mass $m^* = (0.013 \pm 0.001)m$, and the resonance was isotropic

Facing Page 35

FIGURE 8

HALL MOBILITY CURVES

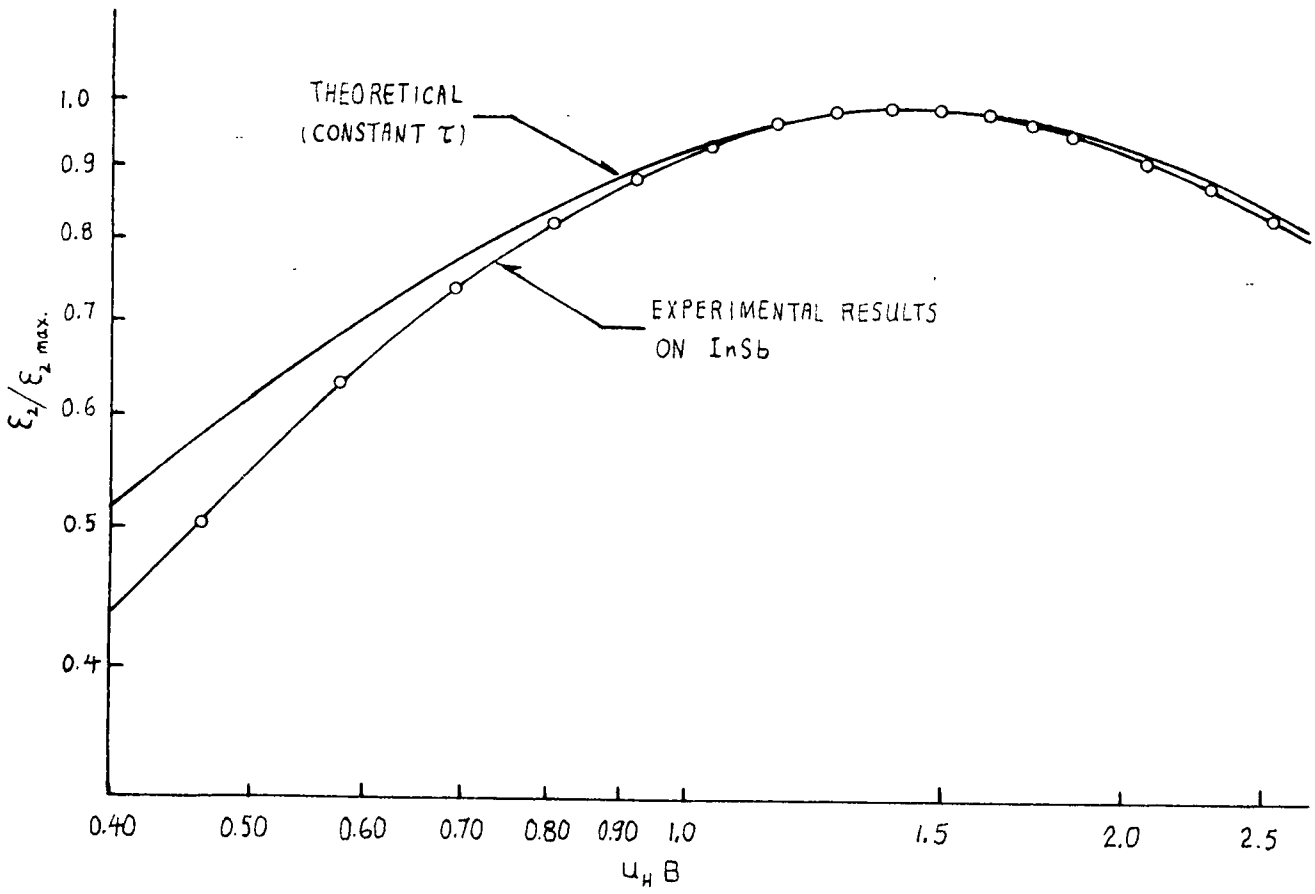

under rotation in a (100) plane, to within experimental error. It is inferred from the isotropic mass that the resonance is associated with conduction electrons. Preliminary observations on two resonance lines with heavier masses $m^* = 0.18m$ and $m^* > 1.2m$, and which show anisotropic behaviour have been made. It is suggested that they may be associated with holes. Hence for n-type indium antimonide it appears to be justifiable to take $K = 1$.

The experimental mixed magnetoresistance curve at high fields cannot be explained because it does not appear to saturate. The longitudinal magnetoresistance component should be zero since the assumption $K = 1$ is satisfied according to Dresselhaus et al (1955). In addition the transverse magnetoresistance curve of Fig. 6 appears to fit the $K = 1$, $\tau \propto (\text{energy})^{-\frac{1}{2}}$ assumptions.

(c) Hall Mobility Measurements. Hall mobilities were measured by the electrodeless technique and by a dc 4-electrode technique.

(i) Crossed Magnetic Field Technique. The static field B_x, is parallel to the plane of the eddy currents. The procedure and apparatus were described in 2.2. In particular,

$$\frac{\mathcal{E}_2}{\mathcal{E}_1} = \left(\frac{1}{Q_{s2}} - \frac{1}{Q_{o2}}\right) \cdot \frac{m_1 L_2}{m_2 L_1} \cdot \frac{(u_H B_x)/2}{1 + (u_H B_x)^2/2} \,. \qquad (22)$$

Hence

$$\mathcal{E}_2 = d \, \frac{u_H B_x}{1 + (u_H B_x)^2/2} \,,$$

where

$$d = \left(\frac{1}{Q_{s2}} - \frac{1}{Q_{o2}}\right) \cdot \frac{\mathcal{E}_1 m_1 L_2}{2 m_2 L_1} \,.$$

In Fig. 8, the experimental pickup voltage $\mathcal{E}_2$ is plotted against B_x, and $\frac{d\, u_H B_x}{1+(u_H B_x)^2/2}$ is plotted against $u_H B_x$. Now the theoretical $\mathcal{E}_2(B_x)$ will be a

maximum when $u_H B_x = \sqrt{2}$ and if the theoretical and experimental curves in Fig. 8 are compared to determine B_x at $\mathcal{E}_{2\,MAX.}$, then u_H may be determined. The maximum occurs at $B_x = 0.315$ W m^{-2}, hence $u_H = 4.5$ m^2 v^{-1} sec^{-1}.

At low fields, one may neglect terms in $(u_H B_x)^2$ and (22) becomes

$$u_H = \frac{2\mathcal{E}_2}{B_x \mathcal{E}_1} \cdot \frac{m_2 L_1}{m_1 L_2} \cdot \frac{Q_{o2} Q_{s2}}{Q_{o2} - Q_{s2}} .$$

The experimental data gave:

$L_1 = 7.5\ \mu$h $n_1 = 40$ turns m^{-1}

$L_2 = 15\ \mu$h $n_2 = 7.7\times10^2$ turns m^{-1}

$\mathcal{E}_1 = 10.8$ v $\mathcal{E}_2 = 10.0$ mv

$Q_{o2} = 66.8$ $Q_{s2} = 18.5$

$B_x = 0.10$ W m^{-2}

Hence $u_H = 4.6$ m^2 v^{-1} sec^{-1}.

(ii) 4-Electrode Hall Constant Measurements. The standard method in which current electrodes are attached to the ends of the sample and 2 potential probes are placed along the sample is used. Now

$$R_H = \frac{E_y}{J_x B_z},$$

where $E = \mathcal{E}/l_1$, l_1 = distance between potential probes, $J_x = I/A_x$, A_x = cross-sectional area of sample perpendicular to direction of I, and

$$u_H = R_H \sigma = \frac{\sigma A_x \mathcal{E}}{l_1 B_z I}.$$

The experimental data are:

$A_x = 1.0$ cm $l_1 = 0.93$ cm $\mathcal{E} = 1.2$ mv

$B_z = 0.14$ W m^{-2} $I = 0.50$ amp and $\sigma = 2.2\times10^4$ mho m^{-1}

Hence $u_H = 4.1$ m^2 v^{-1} sec^{-1}.

(iii) Discussion of Results. There is an error of approximately 10% between the results of (i) and the results of (ii). However experimental errors will account for this discrepancy. In particular, the 4-electrode method involves errors in measuring the dimensions because of the irregular shape of the sample, and end effects will tend to decrease the observed value of u_H because the equipotential surfaces are disturbed. B_z will also vary a few percent over the sample. There are undetermined errors in the crossed magnetic field technique when using the constant collision relaxation time assumption. The transverse magnetoresistance results in (b) indicated that a constant mean free path assumption better fitted the experimental results. This assumption would lead to a different conductivity tensor (E17) and would modify (22) so as to give different results for u_H.

PART II: DIMORPHIC PHASE TRANSFORMATIONS IN COMPOUND SEMICONDUCTORS

CHAPTER 1 - INTRODUCTION

An interesting group of compound semiconductors are the silver salts silver selenide, silver telluride and silver sulfide. They undergo changes in crystalline structure in the temperature range 100 - 200° C. The electrical conductivity and charge carrier density undergo discontinuous changes at the transition due to changes in band structure. A major obstacle to applying conventional dc 4-electrode techniques to determine conductivities and Hall constants is that these compounds are at present available commercially only in the form of powders. It is impossible to attach electrodes to a powder sample and in addition the powder will exhibit an indeterminate bulk conductivity due to intergranular resistance. Consequently an electrodeless technique would appear to be essential.

It is of historical interest to note that silver sulfide is probably the first semiconductor to be discovered. The original reference appears in Faraday's Diary on February 21, 1833. Faraday noticed that on passing a current through a tube of fuzed silver sulfide that "the heat rose as the conducting power increased", indicating that the material had a positive temperature coefficient of conductivity. He also observed the abrupt increase of conductivity at the phase transition.

Experimental work was done on silver selenide powder. This compound exists in two crystalline phases, a low temperature β phase in which the crystal is face-centered tetragonal, and a high temperature α phase in which the crystal is body-centered cubic. Transition temperatures of 122 and 133°C have been reported in Hansen (1958).

The electrodeless techniques of part I were employed in attempts to measure the electronic properties. The temperature variation of conductivity, activation energies, the approximate relative change in conductivity at the phase transition, and a conductivity versus temperature hysteresis effect were observed. Absolute conductivity values could not be obtained because of lack of knowledge of r_i, the radii of the individual particles. The Hall mobility appeared to be much lower than values quoted in the literature indicating that the powder was impure and only impurity scattering was being measured.

Busch and Junod (1957) have prepared silver selenide of known stochiometric ratio by fusion of the components in a quartz crucible. The compound was then purified by zone refining. Measurements of the Hall constant and the electrical conductivity between the temperatures of liquid air and 500°C showed that the type of conductivity in the two crystalline phases was different. They found that in the low temperature phase silver selenide is a semiconductor with activation energy $\Delta E = 0.075$ ev. At 20°C the conductivity was 10^5 mho m^{-1} and the Hall constant was 2×10^{-6} m^3 $coul^{-1}$. The transition between the two crystalline phases occured at 133°C. In the high temperature phase the elementary cell contracted, the electrical conductivity suddenly increased and its variation with temperature became comparable with that of a metal. The charge carrier density increased by a factor of 3 and was constant to temperatures in excess of 300°C. The charge carrier mobility was approximately 0.20 m^2 $v^{-1}sec^{-1}$ at the transition and decreased in proportion to 1/T with increasing temperature. Magnetoresistance measurements showed that the conductivity was electronic, there being negligible measureable ionic conductivity.

Miyatani (1959) has observed results which tend to confirm Busch's results with regard to the mode of conductivity. His results for the electronic conductivity, σ_e, and the ionic conductivity, σ_i, of silver selenide at the transition temperature are:

β phase - $\sigma_e = (2 - 5)\times 10^5$ mho m^{-1}

$\sigma_i = (5 - 20)$ mho m^{-1}

α phase - $\sigma_e = (2 - 5)\times 10^5$ mho m^{-1}

$\sigma_i = 4\times 10^2$ mho m^{-1}

Ranges of conductivity are quoted since according to Miyatani the value is dependent on composition. Miyatani also states that the material is n-type, with an electron mobility $u_m = 0.15$ m^2 v^{-1} sec^{-1} and an effective electron mass of 0.11 m at 124°C. The transition temperature is given as approximately 140°C.

Miyatani (1958) has discussed the effect of the stoichiometric ratio on the transition temperature of silver telluride. The results are given here as they may explain the conductivity versus temperature hysteresis observed for silver selenide. In particular, the transition temperature $T_{\alpha\rightarrow\beta}$ is lowered with increasing deficiency of silver, while the β to α transition temperature $T_{\beta\rightarrow\alpha}$ changes very little. The electronic conductivity also decreases rapidly with small deficiencies of silver and the change of σ_e at the α to β transition is very slow. The slowness of the α to β transition may be due to the precipitation of tellurium, while at the β to α transition it is necessary to heat the specimen to higher temperatures for the precipitated tellurium to reenter the matrix.

CHAPTER 2 - EXPERIMENTAL TECHNIQUES

2.1 Eddy Current Losses in Powders

(a) Theory. The theory for eddy current losses in powders differs somewhat from that for a homogeneous material. In particular, it is important to know whether the eddy currents are confined to the individual particles by high intergranular resistance, or whether they are free to flow across the particle boundaries.

Consider a semiconducting powder made up of Z identical, close-packed, spherical particles of radius r_i. They are imbedded in a lossless medium of permittivity ϵ_o and permeability μ_o so that they are electrically insulated from each other. The density of particles, N, is assumed to be uniform. A uniform sinusoidally varying magnetic field, H_{zo}, is applied and the frequency is low, that is $br_i \leq \frac{1}{2}$. The eddy currents in the individual particles may then be represented by the low frequency formula and the interaction between particles in terms of the induced magnetic dipole moment in individual particles. The total field seen by a particle due to the exciting field and to the secondary field due to all the other particles is then,

$$H' = \frac{H_{zo}}{\left\{1 + j\frac{(br_i)^2}{30} v_i N\right\}}, \qquad (C11)$$

where $v_i = \frac{4\pi r_i^3}{3}$.

Now $v_i N = K_s = \frac{\text{volume occupied by the particles}}{\text{volume of container}} < 1$, hence it is evident that for $br_i \leq \frac{1}{2}$, the secondary magnetic field seen by a particle

due to all the other particles is negligible. Thus there is no interaction between the particles and the total power loss will be the sum of the individual particle power losses. Hence

$$\Delta R = \sum_{i=1}^{Z} \Delta R_i , \tag{1}$$

where, from (B7) and (B8), $$\frac{\Delta R_i}{\omega L_o} = K_{si} \frac{(b r_i)^2}{10} . \tag{2}$$

and Z = number of particles. Finally

$$\frac{\Delta R}{\omega L_o} = K_s \frac{b^2 \langle r_i^2 \rangle}{10} = K_s \frac{(b r_i)^2}{10} , \tag{3}$$

where $$K_s = \frac{4 Z \langle r_i^5 \rangle}{3 r_c^2 l_c \langle r_i^2 \rangle} = \frac{4 Z r_i^3}{3 r_c^2 l_c} . \tag{4}$$

and r_c = radius and l_c = length of solenoid.

The determination of the conductivity of a powder from (3) is seen to involve two serious experimental difficulties. First of all, one would require that the inter-granular conductivity be negligible compared to the conductivity of the individual grains. Secondly the size of the particles must be known, which practically requires that all the grains be of uniform size.

The temperature variation of conductivity may however be studied

since $$\frac{\Delta R}{\omega L_o} = \left(\frac{K_s \mu_o \omega r_i^2}{10} \right) \sigma(T) \tag{3}$$

$$\propto \sigma(T) ,$$

where the constant of proportionality is independent of temperature. An experimental difficulty is that agglomeration or crumbling of particles

may occur, thus changing the constant. Relative conductivities at solid state phase transitions may also be determined if the change in r_i, due to shrinking or expanding of the crystal structure, is small.

(b) Design Considerations. Consider an aggregate of Z identical conducting spherical particles, of radius r_i, which are insulated from each other. The same design formula as were established in I 2.1 apply again for powders with the exception that the critical radius is now r_i, the radius of the individual particles, rather than r_o, the overall radius of the sample.

Thus the optimum frequency defined by $br_i = (\omega_o \sigma \mu_o)^{\frac{1}{2}} r_i = \frac{1}{2}$ is given by

$$f_o = \frac{1}{8\pi\sigma\mu_o r_i^2}, \tag{5}$$

and the low frequency limit from (5) as

$$f_L\sigma = \frac{5}{\pi\mu_o r_i^2 K_s Q_o}, \tag{6}$$

where

$$K_s = \frac{4 r_i^3 Z}{3 r_c^2 l_c} \tag{7}$$

$$= \frac{\text{total volume of particles.}}{\text{volume of solenoid}}$$

Note that the volume of the particles is not the volume of the container since there will be a certain percentage of voids.

The optimum value of inductance for the solenoid is given as in I 2.1c by

$$L_M = \frac{1}{\omega_o^2 C_m}, \tag{8}$$

and the maximum number of turns by

$$N_M = \frac{1}{2\pi r_c f_o}\left(\frac{l_c}{\mu_o \pi C_m}\right)^{\frac{1}{2}}. \tag{9}$$

where C_m is the minimum value of the tuning capacitance of the Q-meter, f_o is given by (5), and r_c = radius and l_c = length of solenoid.

The displacement current limit to the frequency is unchanged at

$$\frac{f}{\sigma} \leq \frac{1.80 \times 10^8}{\epsilon_r} \quad ohm\ m\ sec^{-1} \tag{10}$$

where ϵ_r = relative dielectric constant of the material.

(c) Description of Apparatus. The cylindrical glass sample containers fit coaxially inside the solenoids which are also wound on glass forms. The sizes of these and the optimum values of inductance were discussed in the previous section. Glass was used for these containers and forms because of its low dielectric loss, mechanical stability at temperatures up to 600°C, relative chemical inactivity and also because of the transparency allowing visual observation of the sample to be made.

A special feature of the sample container, which is closed at one end and has a removeable top for adding the sample at the other end, is a small capillary extending from the closed end of the container up the center to the midpoint of the container. One end of a thermocouple is placed in this capillary where it comes in good thermal contact with the sample.

The solenoids are wound using Teflon insulated wire. Teflon is very useful as insulation since it retains all its insulating properties at temperatures in excess of the 200°C temperatures achieved in this experiment.

The Q-meter used was described in I 2.1b and Fig. 2 and 3. The temperature was controlled by placing the solenoid with sample in an oil

bath. Heating and stirring of the oil acheived the necessary degree of temperature control. The oil used was a special insulating oil, Aroclor 1254, which can be used at temperatures up to 300°C. Aroclor 1254 is one of a group of oils composed of chlorinated biphenyl and chlorinated polyphenyls and it should be noted that at temperatures in excess of 100°C the fumes from the oil are very irritating to the skin and arrangements should be made to remove the fumes. The oil bath container was a 1000 ml beaker. The heater was a 100 ohm 5-watt power resistor supplied through a General Radio 5 amp 115 v Variac. The stirring motor, an Eastern Engineering Co., Variable Speed Stirrer, Model 4, 110 v dc or ac, was also supplied through a similar variac. Heating and cooling rates were varied by manipulation of the heating power and stirring rate.

Radiation and convection heat losses were lowered by wrapping the beaker with ¼ in. of corrugated cardboard and by placing a wooden cover on the beaker. The cover also prevented the oil vapors from escaping and it was used to anchor the top of the solenoid, the stirrer shaft, a thermometer, a thermocouple wire and the heater lead-in wires. It would have been possible to obtain much better temperature regulation if a Dewar flask and a better method of temperature regulation had been used. However, the Dewar flask has a serious fault in that eddy currents are induced in the silver layers on its walls, thus greatly reducing the Q of the solenoid. Special Dewar flasks in which the silver layers are interrupted by vertical gaps to prevent the flow of the eddy currents would minimize this effect. These experimental sophistications were not employed however, since very sharp transitions were observed in silver selenide using the experimental techniques described in the previous paragraph.

In making a run the following general procedure was used. The heating power was gradually increased so as to just offset radiation losses. In this way heating rates of $1^{\circ}C$ per minute or lower were attained. The power required by the stirrer decreased with increasing temperature as the viscosity of the oil decreased rapidly. Two temperatures were recorded, the thermometer reading the oil bath temperature and the thermocouple reading the temperature in the sample core, (there being only a small temperature gradient through the walls of the capillary). In this way it was possible to see more easily the cooling or heating rates by noting the temperature gradient between sample and oil bath. In addition a time log of temperature and Q readings was kept. When the sample was well above the transition temperature the heating power was gradually decreased, so as to keep it slightly below the radiation losses, and a cooling run made. A calibration run was also made with the coil alone to determine the variation of Q_o with temperature.

2.2 Hall Mobility Measurements on Powders

The Hall mobility, u_H, is given in the low frequency $br_i \leq \frac{1}{2}$, low field $(u_H B)^2 << 1$, limit by

$$u_H = \frac{2\mathcal{E}_2}{B_x \mathcal{E}_1} \cdot \frac{n_2 L_1}{n_1 L_2} \cdot \frac{Q_{s2} Q_{o2}}{Q_{o2} - Q_{s2}} \qquad \text{I-(22)}$$

where $\mathcal{E}_1$ = voltage on exciting coil of inductance L_1 and n_1 turns/m,

$\mathcal{E}_2$ = voltage on detection coil of inductance L_2 and n_2 turns/m,

B_x = magnetic field applied orthogonally to both coils,

Q_{s2} = Q of detection coil with sample,

Q_{o2} = Q of detection coil without sample,

and r_i = radius of individual particles.

This result is thought to be independent of the shape and the size of the individual particles because it depends on the rotation of the planes of the eddy current which is proportional to $u_H B$. The result is also independent of conductivity and frequency. The technique should prove to be very valuable since there are no other experimental techniques which can be applied in general to powders. For instance, the standard dc 4-electrode technique will not work if the powder exhibits no dc conductivity.

The design considerations are much the same as those for a monocrystal as given in I 2.2b except that, if the eddy currents are confined to individual particles, then the optimum frequency is given by

$$f_0 = \frac{1}{8\pi\sigma\mu_0 r_i^2} \qquad (11)$$

The apparatus is described in I 2.2c.

FIGURE 9

TEMPERATURE VARIATION OF CONDUCTIVITY FOR SILVER SELENIDE

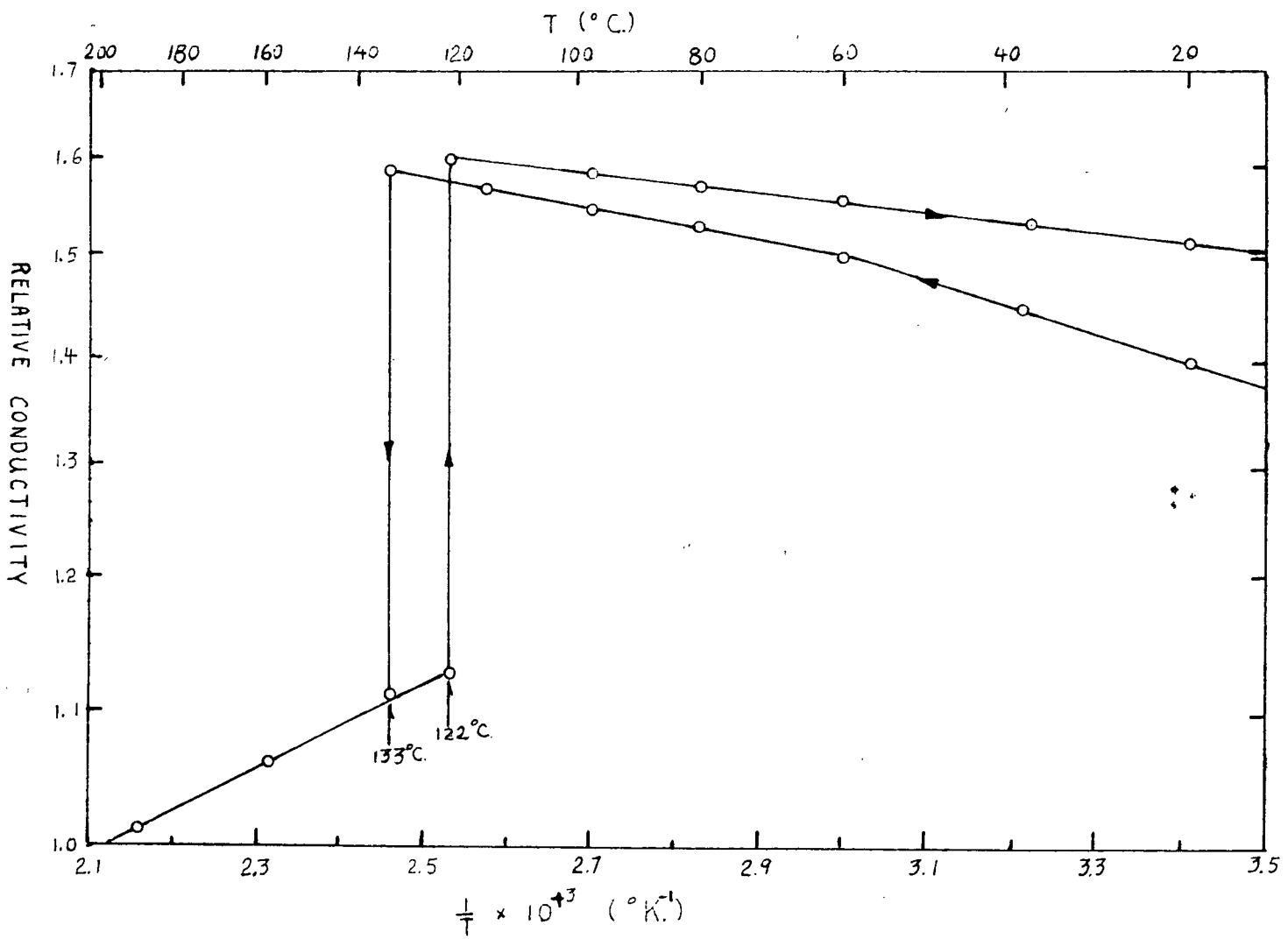

Facing Page 48

CHAPTER 3 - EXPERIMENTAL RESULTS

3.1 Electrical Conductivity of Silver Selenide

The experimental results $1/Q_1 - 1/Q_o$ versus $1/T$ are plotted in Fig. 9. The results may be interpreted in two ways:

(a) If the individual grains of powder are insulated from each other and assumed to be of uniform radius r_i, then

$$\frac{\Delta R}{\omega L_o} = K_s \frac{(br_i)^2}{10} = \frac{1}{Q_1} - \frac{1}{Q_o} \qquad (3)$$

where $K_s = \frac{\text{total volume of particles}}{\text{volume of solenoid}}$, and if $br_i \leq \frac{1}{2}$.

The experimental data gave:

(i) length of solenoid, $l_c = 10.2$ cm,

radius of solenoid, $r_c = 1.35$ cm,

overall length of sample, $l_o = 9.3$ cm,

overall radius of sample, $r_o = 0.72$ cm,

and filling factor of sample container, $F = 0.47$,

giving $K_s = \frac{r_o^2 l_o}{r_c^2 l_c} = 0.12$.

(ii) Q-meter

$T = 50^\circ C$, $f = 3.9 \times 10^5$ cps and $1/Q_1 - 1/Q_o = 4.0 \times 10^{-2}$.

Substituting the data in (3), one obtains $br_i = 1.8$, and hence (3) is not valid. On the basis of estimated values for r_i and σ, it was expected that $br_i \leq \frac{1}{2}$ would be satisfied if this interpretation was true. In particular using $\sigma = 2 \times 10^5$ mho m^{-1}, $r_i = 0.5\ 10^{-3}$ m and $f = 3.9 \times 10^5$ cps, one obtains $br_i = 0.39$.

(b) If the intergranular resistance is assumed to be low so that the current can flow across particle boundaries, then the monocrystalline cylinder formula applies approximately, if allowance is made for voids. The experimental data give as in (a): $K_s = \frac{\text{total volume of particles}}{\text{volume of solenoid}}$ = 0.12, $1/Q_1 - 1/Q_0 = 4.0\times10^{-2}$, and $br_0 > \frac{1}{2}$.

Hence using the general formula (A16),

$$\frac{1}{Q_1} - \frac{1}{Q_0} = \frac{\Delta R}{\omega L_0} = -K_c \, Im\, Y,$$

where
$$-Im\, Y = \frac{2}{br_0}\left\{\frac{ber_0(br_0)\,ber_0'(br_0) + bei_0(br_0)\,bei_0'(br_0)}{ber_0^2(br_0) + bei_0^2(br_0)}\right\}, \quad \text{(A16)}$$

substituting in (A16), one obtains, Im Y = 0.31, and from Fig. 1, $br_0 = 1.8$. Now for $f = 3.9\ 10^5$ cps and $r_0 = 0.72$ cm, $\underline{\sigma = 2.2\times10^4 \text{ mho m}^{-1}}$.

This value for σ can only be considered an estimate of the order of magnitude because of the assumptions made in the calculation. It is in fact about one order of magnitude smaller than the values of $(1 - 5)\times10^5$ mho m^{-1} given by Busch (1957) and Miyatani (1959).

Among the many sources of error, there are:

(a) Fringing of the exciting magnetic field, due to the long solenoid approximation not being satisfied, results in too low a value of observed conductivity.

(b) Disruption of the eddy current patterns at the ends of the sample, an error which would decrease as the length to radius ratio of the sample container was increased, would result in too low a value of observed conductivity.

(c) Errors in measuring the dimensions of the solenoid and the sample container will lead to errors in the conductivity.

(d) There may be pockets of powder insulated from the rest of the sample, thus lowering the observed conductivity.

(e) There is difficulty in defining the current density due to irregular packing of the particles.

(f) The percentage of voids may change and crumbling or agglomeration of particles may take place during the experiment.

(g) Small deviations from stoichiometric ratio lead to a large decrease in conductivity if Miyatani's results on silver telluride, mentioned in the introduction, apply to silver selenide.

On observing the experimental σ versus 1/T curve in Fig. 9, it is seen that in the β phase, $d\sigma/dT$ is positive and hence silver selenide is a semiconductor. Letting $\sigma = \sigma_0 e^{-\frac{\Delta E}{kT}}$, define the activation energy ΔE which may be estimated from the experimental data, one obtains:

(a) Heating run $$\frac{\sigma_1(120^\circ C)}{\sigma_2(20^\circ C)} = \frac{2.06}{1.83},$$

giving $$\Delta E = \frac{\ln(\sigma_1/\sigma_2)}{\frac{1}{k}\left(\frac{1}{T_2} - \frac{1}{T_1}\right)}$$

$$= 0.012 \text{ ev.}$$

(b) Cooling run $$\frac{\sigma_1(120^\circ C)}{\sigma_2(20^\circ C)} = \frac{2.12}{2.00},$$

giving $$\Delta E = 0.0057 \text{ ev.}$$

The value of the activation energy and of the conductivity at a given temperature were observed to change as experiments progressed. This could indicate that on heating the sample some of the volatile selenium evaporated, changing the stoichiometric ratio, since the work

of Miyatani (1958) on silver telluride indicates that the electronic conductivity is very sensitive to small deviations in composition. It is also observed that this value of activation energy is much smaller than the value of 0.075 ev reported by Busch (1957).

In the α phase, $d\sigma/dT$ is negative, thus silver selenide shows metallic behaviour. In particular, if $\sigma \propto T^{\gamma}$, one can calculate a value for γ, from the experimental data. The experimental data give:

$$\frac{\sigma_1(122^\circ C)}{\sigma_2(190^\circ C)} = \frac{1.48}{1.34},$$

giving

$$\gamma = \frac{\ln(\sigma_1/\sigma_2)}{\ln(T_1/T_2)}$$

$$= -0.63.$$

For metallic behaviour $\gamma = -1$.

Two definite transition temperatures were observed, $T_{\alpha \to \beta} = 121^\circ C$ and $T_{\beta \to \alpha} = 133^\circ C$. Busch (1957) reported the transition temperature as $133^\circ C$ and Miyatani (1959) as approximately $140^\circ C$, indicating that they performed only heating experiments on silver selenide. Both transition temperatures have been reported in Hansen. The experimental cooling and heating rates were as slow as $1^\circ C$ per minute. Miyatani (1958), in experiments on silver telluride, has found that $T_{\alpha \to \beta}$ is lowered by small deficiencies of the silver component while $T_{\beta \to \alpha}$ is relatively unaffected. The similarity of silver selenide and silver telluride indicates that this phenomena may also take place in silver selenide, thus explaining the hysteresis effect.

At the β toα transition a discontinuous decrease in conductivity takes place. In particular, neglecting volume changes,

$$\frac{\sigma_\alpha}{\sigma_\beta} = \frac{1.46}{2.08} = 0.70,$$

a 30% decrease in conductivity. Busch (1957) states that the conductivity increases suddenly at the β to α transition. Again, appealing to the work of Miyatani (1959), the disagreement in results may be due to differences in composition.

3.2 Hall Mobility Measurements on Silver Selenide

Attempts were made to measure the Hall mobility of silver selenide, using the electrodeless technique described in 2.2. The results were not consistent. In particular, two typical experiments gave:

		(i)	(ii)
$\mathcal{E}_1$	(v)	10.3	11.7
n_1	(turns m^{-1})	80	80
L_1	(μh)	30	30
$\mathcal{E}_2$	(mv)	0.40	0.055
n_2	(turns m^{-1})	1.6×10^3	10^3
L_2	(μh)	27	105
B_x	(W m^{-2})	0.45	0.34
Q_{s2}		5.96	34.0
Q_{o2}		57.3	74.5
f	(Mc)	1.0	0.50
T	(°C)	20	20
u_H	(m^2 v^{-1} sec^{-1})	0.025	0.0062

Busch (1957) gave $u_m = 0.20$ m^2 v^{-1} sec^{-1} at 20°C and Miyatani (1959) gave $u_m = 0.15$ m^2 v^{-1} sec^{-1} at 125°C for the electron mobility of silver selenide. The most likely explanation for the low values of u_H obtained in this experiment is that the sample was relatively impure and hence only impurity scattering was being measured. In particular, for neutral impurity scattering Erginsoy (1950) gives, for the impurity concentration,

$$N_D = \frac{m^* e^3}{20 u_m \epsilon \hbar^3} .$$

Hence, using $u_m = 0.015\ m^2\ v^{-1}\ sec^{-1}$, $m^* = 0.11m$ (from results of Miyatani) and $\epsilon = 5\epsilon_o$; $N_D = 2.6 \times 10^{25}\ m^{-3}$, which corresponds to an impurity concentration of 0.16%, which would be considered chemically pure but not electronically pure.

The problem of error signals is very severe on low mobility materials. From I - (30), the error due to small angular deviation, θ , from orthogonality, of the exciting and pickup coils is given approximately by

$$\frac{\mathcal{E}_e}{\mathcal{E}_2} = \frac{1.1\,\theta^\circ}{u_H B_x} ,$$

where $\mathcal{E}_e$ = error voltage due to pickup from exciting coil,

and $\mathcal{E}_2$ = voltage due to Hall effect.

Now for $u_H = 0.015\ m^2\ v^{-1}\ sec^{-1}$, $B_x = 0.50\ W\ m^{-2}$ we see that for a $\frac{1}{2}^\circ$ misalignment $\mathcal{E}_e / \mathcal{E}_2$ is 73.

APPENDIX A

Change in Resistance and Inductance of a Solenoid due to a Conducting Cylindrical Core

Let the sample of conductivity σ, permittivity ϵ, and permeability μ be homogeneous and isotropic. MKS units are used throughout. The sample is in the form of a long cylinder of radius r_o and length l_o. Eddy currents are induced in the sample by the magnetic field B_{zo} of the solenoid and a resistance accordingly reflected back into the solenoid. At high frequencies the magnetic field is unable to penetrate the sample resulting in a decrease in inductance of the solenoid. The effects will be calculated specifically. The solenoid is of radius r_c and length l_c, where $l_c > l_o$ and l_c is large compared to r_c so that the field inside the solenoid is uniform and axial. The magnetic field and current density inside the sample are calculated by solving Maxwell's equations. All time varying quantities are sinusoidal.

The relation $\vec{J} = \sigma \vec{E}$ and the transformation $d/dt = j\omega$ substituted in Maxwell's equations gives

$$\nabla \times \vec{H} = \vec{J} + \frac{\partial \vec{D}}{\partial t} = \vec{J}\left(1 + j\frac{\omega\epsilon}{\sigma}\right), \tag{A1}$$

and

$$\nabla \times \vec{J} = -j\omega\sigma\mu\,\vec{H}. \tag{A2}$$

Substitution of (A2) in (A1) gives

$$\nabla \times (\nabla \times \vec{H}) = -j\,\omega\sigma\mu\,\vec{J}\left(1 + j\frac{\omega\epsilon}{\sigma}\right).$$

But

$$\nabla \times (\nabla \times \vec{H}) = -\nabla^2 H.$$

Hence $$\nabla^2 \vec{H} = j b^2 \left(1 + j \frac{\omega \epsilon}{\sigma}\right) \vec{H}, \tag{A3}$$

where $$b^2 = \omega \sigma \mu .$$

Assume that:

(a) displacement currents are negligible, i.e. $\frac{\omega \epsilon}{\sigma} << 1$,

(b) circular symmetry and infinite length, i.e. $\frac{\partial}{\partial \phi} = 0 = \frac{\partial}{\partial z}$.

(c) $H(r) = H(r)\vec{z}_o$, where $\vec{z}_o$ = unit vector in the z-direction.

Thus $$\nabla^2 H \, \vec{z}_o = -j b^2 H \, \vec{z}_o ,$$

giving $$\frac{1}{r} \frac{d}{dr}\left(r \frac{dH}{dr}\right) = -j b^2 H. \tag{A4}$$

Substitute $x = j^{\frac{3}{2}} br$ in (A4) and obtain,

$$\frac{d^2 H}{dx^2} + \frac{1}{x} \frac{dH}{dx} + H = 0. \tag{A5}$$

The solutions of (A5) are the Bessel functions, $J_o(x)$ and $Y_o(x)$.

Hence $$H(r) = A J_o(x) + B Y_o(x).$$

The boundary conditions are:

(a) $H(r = 0)$ is finite,

(b) $H(r = r_o) = H_{zo}$, by Stokes theorem.

Thus $$H(r) = H_{zo} \frac{J_o(x)}{J_o(x_o)} ,$$

since $Y_o(0)$ is infinite, and where $x_o = j^{\frac{3}{2}} br_o$.

The complex function $J_o(x)$ may be separated into real and imaginary parts

using, $$J_o(x) = ber_o(br) + j \, bei_o(br). \tag{A6}$$

Thus $$H(br) = H_{zo} \frac{ber_o(br) + j \, bei_o(br)}{ber_o(br_o) + j \, bei_o(br_o)} , \tag{A7}$$

and
$$J(br) = -\frac{dH}{dr}$$
$$= b H_{z0} \frac{ber_0'(br) + j\, bei_0'(br)}{ber_0(br_0) + j\, bei_0(br)} . \qquad \text{(A8)}$$

Calculation of the total complex flux, Φ, through the sample determines the impedance reflected into the solenoid. Thus

$$\Phi = N \int_{Area} \vec{B} \cdot d\vec{A} , \qquad \text{(A9)}$$

where N = total turns of solenoid linking the sample,

= nl_0, where n = turns/m on solenoid.

If (A7) is substituted in (A9), then

$$\Phi = \frac{\mu_0 m N i}{ber_0(br_0) + j\, bei_0(br_0)} \int_0^r \int_0^{2\pi} \left\{ ber_0(br) + j\, bei_0(br) \right\} r\, dr\, d\phi$$

$$= i K_c L_0 Y , \qquad \text{(A10)}$$

where
$$Y = \frac{2}{br_0} \left\{ \frac{bei_0'(br_0) - j\, ber_0'(br_0)}{ber_0(br_0) + j\, bei_0(br_0)} \right\}, \qquad \text{(A11)}$$

$$L_0 K_c = \mu_0 m^2 \pi r_0^2 l_0 ,$$

$L_0 = \mu_0 m^2 \pi r_c^2 l_c$ = inductance of solenoid without the sample, (A12)

and
$K_c = \frac{r_0^2 l_0}{r_c^2 l_c}$ = filling factor of solenoid. (A13)

Hence the complex change in inductance of the solenoid

$$= \frac{\Phi - \Phi_0}{i}$$

$$= K_c (Y - 1) L_0$$

$$= \Delta L + \frac{\Delta R}{j\omega} \qquad \text{(A14)}$$

Thus
$$\frac{\Delta L}{L_o} = -K_c \, Re\,(1 - Y)$$
$$= -K_c \left\{ 1 - \frac{2}{br_o} \left[\frac{bei_o'(br_o)\, ber_o(br_o) - ber_o'(br_o)\, bei_o(br_o)}{ber_o^2(br_o) + bei_o^2(br_o)} \right] \right\}, \quad \text{(A15)}$$

and
$$\frac{\Delta R}{\omega L_o} = -K_c \, Im\, Y$$
$$= K_c \frac{2}{br_o} \left\{ \frac{ber_o(br_o)\, ber_o'(br_o) + bei_o(br_o)\, bei_o'(br_o)}{ber_o^2(br_o) + bei_o^2(br_o)} \right\} \quad \text{(A16)}$$

The limiting forms for small and large arguments of the Bessel functions are now easily determined:

(a) $br_o \leq \frac{1}{2}$

The Bessel functions are given by the series expansions,

$$ber_o(x) = 1 - \frac{\left(\frac{x}{2}\right)^4}{(2!)^2} + \frac{\left(\frac{x}{2}\right)^8}{(4!)^2} - \cdots,$$
$$bei_o(x) = \frac{\left(\frac{x}{2}\right)^2}{(1!)^2} - \frac{\left(\frac{x}{2}\right)^6}{(3!)^2} + \frac{\left(\frac{x}{2}\right)^{10}}{(5!)^2} - \cdots,$$
$$ber_o'(x) = -\frac{\left(\frac{x}{2}\right)^3}{1!\,2!} + \frac{\left(\frac{x}{2}\right)^7}{3!\,4!} - \frac{\left(\frac{x}{2}\right)^{11}}{5!\,6!} + \cdots,$$

and
$$bei_o'(x) = \frac{\left(\frac{x}{2}\right)}{0!\,1!} - \frac{\left(\frac{x}{2}\right)^5}{2!\,3!} + \frac{\left(\frac{x}{2}\right)^9}{4!\,5!} - \cdots \quad \text{(A17)}$$

Substituting (A17) in (A15) and (A16) one obtains,

$$\frac{\Delta L}{L_o} = -K_c \frac{(br_o)^4}{96}, \quad \text{(A18)}$$

and
$$\frac{\Delta R}{\omega L_o} = K_c \frac{(br_o)^2}{8}. \quad \text{(A19)}$$

as the first approximation for the reflected impedance.

(b) br $\geq$ 10

The Bessel functions are given to the first order of approximation by,

$$ber_o(x) = \frac{e^{\frac{x}{\sqrt{2}}}}{\sqrt{2\pi x}} \cos\left(\frac{x}{\sqrt{2}} - \frac{\pi}{8}\right),$$

$$bei_o(x) = \frac{e^{\frac{x}{\sqrt{2}}}}{\sqrt{2\pi x}} \sin\left(\frac{x}{\sqrt{2}} - \frac{\pi}{8}\right),$$

$$ber_o'(x) = \frac{e^{\frac{x}{\sqrt{2}}}}{\sqrt{2\pi x}} \cos\left(\frac{x}{\sqrt{2}} + \frac{\pi}{8}\right),$$

and

$$bei_o'(x) = \frac{e^{\frac{x}{\sqrt{2}}}}{\sqrt{2\pi x}} \sin\left(\frac{x}{\sqrt{2}} + \frac{\pi}{8}\right). \qquad \text{(A20)}$$

Subetituting (A20) in (A15) and (A16) one obtains,

$$\frac{\Delta L}{L_o} = - K_c \left(1 - \frac{\sqrt{2}}{br_o}\right), \qquad \text{(A21)}$$

and

$$\frac{\Delta R}{\omega L_o} = K_c \frac{\sqrt{2}}{br_o}. \qquad \text{(A22)}$$

as the first approximation for the reflected impedance.

APPENDIX B

Change in Inductance and Resistance of a Solenoid due to a Conducting Spherical Core

The sample, a sphere of radius r_o, conductivity σ, permeability μ_o, and permittivity ϵ, is homogeneous and isotropic. The sample is placed in a long solenoid of radius r_c, length l_c, and of n turns/m, and the resistance and inductance changes reflected into the solenoid by the sample are calculated. Hence one must solve equation (A4), in spherical coordinates.

Assume that:

(a) displacement currents are negligible, i.e. $\frac{\omega\epsilon}{\sigma} << 1$,

(b) the magnetic field is not a function of ϕ,

(c) $\overrightarrow{H(r,\theta)} = H(r,\theta)\vec{z}_o$ where $\vec{z}_o$ is a unit vector in the z-direction, and

(d) the frequency is low so that $(\omega\sigma\mu_o)^{\frac{1}{2}} r_o = br_o << 1$.

Since $br_o << 1$, the secondary magnetic fields, outside the sphere are expressible in terms of the equivalent magnetic dipole induced in the sphere. This magnetization $\vec{m}$, is in the $\vec{z}$ direction, and is in general a complex quantity.

Wait (1953), has given the solution to the more general problem where $\mu \neq \mu_o$ and displacement currents are not negligible. Putting $\mu = \mu_o$ and assuming that the displacement currents are negligible one obtains,

$$\vec{m} = -\vec{H}_{zo}(p + jq)V_s, \qquad \text{(B1)}$$

where $V_s = \frac{4\pi r_o^3}{3}$ = volume of sample,

and p and q are real quantities given by

$$p + jq = \frac{3}{2}\left[1 + \frac{3(\sinh\alpha - \alpha\cosh\alpha)}{\alpha^2 \sinh\alpha}\right], \tag{B2}$$

and where $$\alpha = \sqrt{j}\,(\omega\sigma/\mu_o)^{\frac{1}{2}} r_o = \sqrt{j}\, b r_o. \tag{B3}$$

Now since $br_o << 1$,

$$\sinh\alpha = \frac{\alpha}{1!} + \frac{\alpha^3}{3!} + \frac{\alpha^5}{5!} + \ldots,$$

and $$\cosh\alpha = 1 + \frac{\alpha^2}{2!} + \frac{\alpha^4}{4!} + \ldots,$$

and one may simplify (B2) to obtain as the first order terms:

$$p = \frac{(br_o)^4}{105} \tag{B4}$$

and $$q = \frac{(br_o)^2}{10} \tag{B5}$$

Now $-(p + jq)$ = complex magnetization per unit field per unit volume.

Hence $$\frac{\Delta L}{L_o} = -K_s p = -K_s \frac{(br_o)^4}{105}, \tag{B6}$$

and $$\frac{\Delta R}{\omega L_o} = K_s q = K_s \frac{(br_o)^2}{10}, \tag{B7}$$

where $$K_s = \frac{4 r_o^3}{3 r_c^2 l_c} = \frac{\text{volume of sample}}{\text{volume of solenoid}}. \tag{B8}$$

APPENDIX C

The Internal Field in an Array of Conducting Spherical Particles

Consider a uniform array of uniform spherical particles of radius r_i imbedded in a lossless medium of permeability μ_o and permittivity ϵ_o. The particles are close packed and let the density of particles be N. A uniform magnetic field H_{zo} is applied along the axis of the cylinder and the frequency in low so that $br_i = (\omega\sigma\mu_o)^{\frac{1}{2}} r_i << 1$ and hence the secondary field outside the particle due to itself is expressible in terms of the equivalent magnetic dipole that is induced in the spherical particle.

Consider the magnetization of one particle. The dipole moment of the current distribution with respect to the center of the particle is

$$\vec{m} = \frac{\mu_o}{2} \int_{Vol.} (\vec{r} \times \vec{J})\, d\tau \qquad (C1)$$

where $\vec{r}$ = vector directed from the center of the sphere to the current element,

and $$\vec{J} = -j \frac{b^2}{2} H' r \sin\theta \; \vec{\Phi}_o, \qquad (C2)$$

where H' = local field seen by particles.

Now $$\vec{r} \times \vec{\Phi}_o = -r\cos\theta \; \vec{\rho}_o + r \sin\theta \; \vec{z}_o.$$

Hence $$\vec{m} = -j \frac{b^2}{4} \mu_o H' \int_{Vol.} \left\{ r^2 \sin^2\theta \; \vec{z}_o - r^2 \sin\theta \cos\theta \; \vec{\rho}_o \right\} r^2 \sin\theta \, dr \, d\phi \, d\theta.$$

Evaluating the integrals, $$\vec{m} = -j \frac{(br_i)^2}{10} \mu_o H' v_i \vec{z}_o, \qquad (C3)$$

where $$v_i = \frac{4\pi r_i^3}{3},$$

and $\vec{z}_o$ = unit vector in z-direction.

The total magnetization is then, $\vec{M} = N\vec{m}$. (04)

It may be noted that if the particles had a permeability $\mu > \mu_o$, then there would be a static magnetization.

To evaluate the local field, H', seen by a particle, consider a small spherical cavity containing one particle. The particles are assumed to be close packed and hence the magnetization of the material surrounding the cavity may be assumed to be uniform. Stratton (1941), shows that the local field, H', at the center of such a cavity is,

$$\vec{H'} = \vec{H}_{zo} + \frac{\vec{M}}{3\mu_o}. \qquad (05)$$

On substituting for $\vec{M}$ from (03) and (04), one obtains, as the first approximation at low frequency,

$$\vec{H'} = \frac{\vec{H}_{zo}}{1 + j\frac{(b\pi_i)^2}{30} N v_i}, \qquad (06)$$

where $Nv_i = K_s = \frac{\text{total volume of particles.}}{\text{volume of solenoid}}$ (07)

APPENDIX D

The Conductivity Tensor

Consider a particle of mass m and charge q in combined electric and magnetic fields. The fields are constant throughout space and are in arbitrary directions. The magnetic field is static, while the electric field varies sinusoidally. Furthermore assume a collision relaxation time, τ, which is independent of velocity v and that 1/m is a scalar.

The forces on the particle due to the fields are:

$$F_x = q\,(v_y B_z - v_z B_y + E_x),$$

$$F_y = q\,(v_z B_x - v_x B_z + E_y),$$

and $$F_z = q\,(v_x B_y - v_y B_x + E_z). \qquad \text{(D1)}$$

Substitute (D1) in the equations of motion of the particle and obtain:

$$m v_x = j\omega m v_x = q\,(E_x + v_y B_z - v_z B_y) - \frac{m v_x}{\tau},$$

$$j\omega m v_y = q\,(E_y + v_z B_x - v_x B_z) - \frac{m v_y}{\tau},$$

and $$j\omega m v_z = q\,(E_z + v_x B_y - v_y B_x) - \frac{m v_z}{\tau}. \qquad \text{(D2)}$$

where mv_i/τ are the energy loss terms due to collisions.

Introduce the notation

$$\omega_{ck} = \frac{q B_k}{m},$$

$$C_k = \frac{\omega_{ck}}{j\omega + \frac{1}{\tau}},$$

and $$K = -\frac{q\tau}{m}\frac{1}{1+j\omega\tau}.$$

On collecting terms (D2) become

$$V_x - C_z V_y + C_y V_z = K E_x,$$

$$C_z V_x + V_y - C_x V_z = K E_y,$$

and $$-C_y V_x + C_x V_y + V_z = K E_z. \qquad (D3)$$

The solution of (D3) give

$$\frac{D V_x}{K} = (1+C_x^2) E_x + (C_x C_y + C_z) E_y + (C_x C_z - C_y) E_z,$$

$$\frac{D V_y}{K} = (C_x C_y - C_z) E_x + (1 + C_y^2) E_y + (C_y C_z + C_x) E_z,$$

and $$\frac{D V_z}{K} = (C_x C_z + C_y) E_x + (C_y C_z - C_x) E_y + (1 + C_z^2) E_z, \qquad (D4)$$

where $$D = 1 + C_x^2 + C_y^2 + C_z^2$$

$$= 1 + \frac{\omega_c \tau}{1 + j\omega\tau}.$$

The general relations $J_k = n q V_k$ and $J_k = \sigma_{kl} E_l$,

also hold, where n = number of particles per unit volume.

Multiply (D4) by nq and note that $\sigma_o = \frac{nq^2\tau}{m}$, to obtain

$$\frac{D J_x}{\sigma_o(1+j\omega\tau)} = (1+C_x^2) E_x + (C_x C_y + C_z) E_y + (C_x C_z - C_y) E_z,$$

$$\frac{D J_y}{\sigma_o(1+j\omega\tau)} = (C_x C_y - C_z) E_x + (1 + C_y^2) E_y + (C_y C_z + C_x) E_z,$$

and $$\frac{D J_z}{\sigma_o(1+j\omega\tau)} = (C_x C_z + C_y) E_x + (C_y C_z - C_x) E_y + (1 + C_z^2) E_z. \qquad (D5)$$

On comparing coefficients,

$$\sigma = F \begin{pmatrix} 1 + C_x^2 & C_x C_y + C_z & C_x C_z - C_y \\ C_x C_y - C_z & 1 + C_y^2 & C_y C_z + C_x \\ C_x C_z + C_y & C_y C_z - C_x & 1 + C_z^2 \end{pmatrix}, \tag{D6}$$

where $$F = \frac{\sigma_o}{D}(1 + j\omega\tau). \tag{D7}$$

At low frequencies such that $\omega\tau << 1$,

$$F = \frac{\sigma_o}{1 + (\tau\omega_c)^2}, \tag{D8}$$

and $$C_k = \tau\omega_{ck}. \tag{D9}$$

APPENDIX E

Magnetoresistance and Hall Mobility

Consider a long cylindrical or spherical sample of conductivity σ, permittivity ϵ, and permeability μ_o inside a solenoid, as in appendices A or B. Circulating eddy currents are then induced in the sample. A static magnetic field B is applied and the change in resistance of the solenoid, measured as a function of B, is calculated for two specific orientations of the fields. In a third case, the change in resistance of a solenoid placed orthogonally to the exciting and static fields is calculated. The collision relaxation time, τ, is assumed to be constant, and 1/m is assumed to be a scalar and hence the conductivity tensor derived in appendix D may be used.

In order that the results of appendix D may be applied, the equivalent exciting electric field must be determined. Maxwell's equation states that

$$\nabla \times \vec{B} = -\frac{\partial \vec{B}}{\partial t}.$$

Hence
$$\frac{\vec{k_o}}{r\sin\theta}\,\frac{\partial}{\partial(r\sin\theta)}\left(r\sin\theta\, E_\phi\right) = -j\omega B_{zo}\,\vec{k_o}. \tag{E1}$$

The solution of (E1) is,
$$E_\phi = -\frac{j\omega B_{zo} r\sin\theta}{2}. \tag{E2}$$

Thus
$$E_x = -E_\phi \sin\phi = \frac{j\omega B_{zo} y}{2}, \tag{E3}$$

and
$$E_y = E_\phi \cos\phi = -\frac{j\omega B_{zo} x}{2}. \tag{E4}$$

Now assume $\omega\tau \ll 1$ and $\tau\omega_{ck} = \tau q B_k/m$. But $\tau q/m = u_H$, the Hall mobility of the particles, hence $\tau\omega_{ck} = u_H B_k$, $(k = x,y,z)$. (E5)

(1) Transverse Magnetoresistance

The static field B_z is perpendicular to the eddy current planes. The conductivity tensor, (D6), becomes:

$$\sigma = \frac{\sigma_o}{1+(u_H B_z)^2}\begin{pmatrix} 0 & u_H B_z & 0 \\ -u_H B_z & 1 & 0 \\ 0 & 0 & 1+(u_H B_z)^2 \end{pmatrix}. \qquad (E6)$$

Hence the current density,

$$\vec{J} = \left\{\frac{\sigma_o E_x}{1+(u_H B_z)^2} - \frac{u_H B_z \sigma_o E_y}{1+(u_H B_z)^2}\right\}\vec{i} + \left\{\frac{u_H B_z \sigma_o E_x}{1+(u_H B_z)^2} + \frac{\sigma_o E_y}{1+(u_H B_z)^2}\right\}\vec{j}, \qquad (E7)$$

and $$\vec{J}\cdot\vec{E} = \frac{\sigma_o}{1+(u_H B_z)^2}\left\{E_x^2 + E_y^2\right\} = \frac{\sigma_o E_\phi^2}{1+(u_H B_z)^2}. \qquad (E8)$$

The power, W, dissipated in the sample is

$$W = i^2 \Delta R = \frac{\sigma_o}{1+(u_H B_z)^2}\int_{Vol.} |E_\phi|^2 \, d\tau. \qquad (E9)$$

In the low frequency region ($br_o \leq \frac{1}{2}$), substitute (E2) and $B_{z0} = \mu_0 ni$ in (E9) to obtain:

$$\Delta R = \frac{\sigma_o}{1+(u_H B_z)^2}\left(\frac{\mu_0 \omega n}{2}\right)^2 \int_{Vol.} r^2 \sin^2\theta \, d\tau. \qquad (E10)$$

Consider two special cases:

(a) A cylinder of radius r_o and length l_o gives

$$\int_{\rho=0}^{r_o}\int_{z=0}^{l_o}\int_{\phi=0}^{2\pi} \rho^2 (\rho \, d\rho \, dz \, d\phi) = \frac{\pi r_o^4 l_o}{2}.$$

Hence $$\frac{\Delta R}{\omega L_o} = K_c \frac{(br_o)^2}{8}\frac{1}{1+(u_H B_z)^2}, \qquad (E11)$$

where $$L_o K_c = \mu_o n^2 \pi l_o r_o^2, \tag{E12}$$

and $$K_c = \frac{r_o^2 l_o}{r_c^2 l_c}. \tag{E13}$$

(b) A sphere of radius r_o gives

$$\int_{r=0}^{r_o}\int_{\theta=0}^{\pi}\int_{\phi=0}^{2\pi} (r\sin\theta)^2 (r^2 \sin\theta\, dr\, d\theta\, d\phi) = \frac{2}{5} r_o^2 \left(\frac{4\pi r_o^3}{3}\right).$$

Hence $$\frac{\Delta R}{\omega L_o} = K_s \frac{(b r_o)^2}{10} \frac{1}{1+(u_H B_z)^2}, \tag{E14}$$

where $$L_o K_s = \mu_o n^2 \frac{4}{3} \pi r_o^3, \tag{E15}$$

and $$K_s = \frac{4 r_o^3}{3 r_c^2 l_c}. \tag{E16}$$

(2) Mixed Magnetoresistance

The static field B_x is parallel to the eddy current planes. The conductivity tensor, (D6), becomes:

$$\sigma = \frac{\sigma_0}{1+(u_H B_x)^2}\begin{pmatrix} 1+(u_H B_x)^2 & 0 & 0 \\ 0 & 1 & -u_H B_x \\ 0 & u_H B_x & 1 \end{pmatrix}. \qquad \text{(E17)}$$

Hence the current density,

$$\vec{J} = \sigma_0 E_x \vec{i} + \frac{\sigma_0 E_x}{1+(u_H B_x)^2}\vec{j} + \frac{u_H B_x \sigma_0 E_y}{1+(u_H B_x)^2}\vec{k}, \qquad \text{(E18)}$$

and $$\vec{J}\cdot\vec{E} = \sigma_0 E_x^2 + \frac{\sigma_0}{1+(u_H B_x)^2} E_y^2. \qquad \text{(E19)}$$

The power dissipated in the sample is,

$$W = i^2 \Delta R = \sigma_0 \int_{Vol.} \left\{ E_x^2 + \frac{E_y^2}{1+(u_H B_x)^2} \right\} d\tau. \qquad \text{(E20)}$$

In the low frequency region ($br_0 \leq \frac{1}{2}$), substitute (E3), (E4) and $B_{z0} = \mu_0 ni$ in (E20) to obtain:

$$\Delta R = \sigma_0 \left(\frac{\mu_0 \omega n}{2}\right)^2 \int_{Vol.} \left\{ r^2 \sin^2\theta \sin^2\phi + \frac{r^2 \sin^2\phi \cos^2\theta}{1+(u_H B_x)^2} \right\} d\tau \qquad \text{(E21)}$$

The first term in the integral represents the longitudinal component and the second term represents the transverse component of resistance. Note that there is no longitudinal magnetoresistance.

Consider two special cases:

(a) A cylinder of radius r_o and length l_o, and $r\sin\theta = \rho$, gives

$$\int_{\rho=0}^{r_o}\int_{z=0}^{l_o}\int_{\phi=0}^{2\pi}\left\{\rho^2\sin^2\phi + \frac{\rho^2\cos^2\phi}{1+(u_H B_x)^2}\right\}\rho\, d\rho\, dz\, d\phi$$

$$= \frac{\pi l_o r_o^4}{4}\left\{1 + \frac{1}{1+(u_H B_x)^2}\right\}.$$

Hence $$\Delta R = \sigma_o\left(\frac{\mu_o\omega m}{2}\right)^2\frac{\pi l_o r_o^4}{4}\left\{1 + \frac{1}{1+(u_H B_x)^2}\right\},$$

and $$\frac{\Delta R}{\omega L_o} = K_c\frac{(br_o)^2}{8}\left\{\frac{1}{2} + \frac{1/2}{1+(u_H B_x)^2}\right\}, \qquad \text{(E22)}$$

since $$K_c L_o = \mu_o m^2 \pi r_o^2 l_o, \qquad \text{(E12)}$$

and $$b^2 = \omega\sigma\mu_o.$$

(b) A sphere of radius r_o gives

$$\int_{r=0}^{r_o}\int_{\theta=0}^{\pi}\int_{\phi=0}^{2\pi}\left\{r^2\sin^2\theta\cos^2\phi + \frac{r^2\sin^2\theta\sin^2\phi}{1+(u_H B_x)^2}\right\}(r^2\sin\theta\, d\phi\, d\theta\, dr)$$

$$= \frac{r_o^2}{5}\left(\frac{4\pi r_o^3}{3}\right)\left\{1 + \frac{1}{1+(u_H B_x)^2}\right\}.$$

Hence $$\Delta R = \sigma_o\left(\frac{\omega\mu_o m}{2}\right)^2\left(\frac{4\pi r_o^3}{3}\right)\left(\frac{r_o^2}{5}\right)\left\{1 + \frac{1}{1+(u_H B_x)^2}\right\},$$

and $$\frac{\Delta R}{\omega L_o} = K_s\frac{(br_o)^2}{10}\left\{\frac{1}{2} + \frac{1/2}{1+(u_H B_x)^2}\right\}, \qquad \text{(E23)}$$

since $$K_s L_o = \mu_o m^2 \frac{4}{3}\pi r_o^3. \qquad \text{(E15)}$$

(3) Hall Mobility

The static field B_x is parallel to the eddy current planes as in (2).

Hence $$\vec{J} = \sigma_o E_x \vec{i} + \frac{\sigma_o E_y}{1+(u_H B_x)^2} \vec{j} + \frac{u_H B_x \sigma_o E_y}{1+(u_H B_x)^2} \vec{k}. \qquad \text{(E18)}$$

Now, if a second solenoid is set up with axis along the y-direction, its field B_{y2}, equivalent to electric fields

$$E_{x2} = \frac{j\omega B_{y2} z}{2}, \qquad \text{(E24)}$$

and $$E_{z2} = -\frac{j\omega B_{y2} x}{2}, \qquad \text{(E25)}$$

by (E2), will interact with the currents set up by coil 1.

Thus $$\vec{J_1} \cdot \vec{E_2} = \sigma_o E_{x1} E_{x2} + \sigma_o E_{y1} E_{z2} \frac{u_H B_x}{1+(u_H B_x)^2}. \qquad \text{(E26)}$$

Now $R_{21} = V_2/i_1$, the transfer impedance from coil 1 to coil 2, is given by:

$$R_{21} = \frac{1}{i_1 i_2} \int_{Vol.} \vec{J}_1 \cdot \vec{E}_2 \, d\tau$$

$$= \frac{\sigma_o}{i_1 i_2} \int_{Vol.} \left\{ E_{x1} E_{x2} + \frac{u_H B_x}{1+(u_H B_x)^2} E_{y1} E_{z2} \right\} d\tau. \qquad \text{(E27)}$$

In the low frequency region ($br_o \leq \frac{1}{2}$), substitute (E3), (E4), $B_{z1} = \mu_o n_1 i_1$ and $B_{z2} = \mu_o n_2 i_2$ in (E27) to obtain:

$$R_{21} = \frac{\omega b^2 \mu_o n_1 n_2}{4} \left\{ \int_{Vol.} \left[yz + \frac{u_H B_x}{1+(u_H B_x)^2} x^2 \right] dx\, dy\, dz \right\}. \qquad \text{(E29)}$$

Consider two special cases:

(a) A cylinder of radius r_o and length l_o, gives

$$\int_{Vol.} y z \, d\tau = 0 ,$$

and

$$\int_{Vol.} x^2 \, dx \, dy \, dz = \frac{h_o^2}{4} (\pi h_o^2 l_o),$$

Hence

$$R_{21} = \omega \frac{(b h_o)^2}{16} \frac{\mu_H B_x}{1+(\mu_H B_x)^2} \left\{ \mu_o n_1 n_2 \pi l_o h_o^2 \right\}. \qquad \text{(E29)}$$

(b) A sphere of radius r_o, gives

$$\int_{Vol.} y z \, d\tau = 0,$$

and

$$\int_{Vol.} x^2 \, dx \, dy \, dz = \frac{h_o^2}{5} \left(\frac{4 \pi h_o^3}{3} \right),$$

Hence

$$R_{21} = \frac{\omega (b h_o)^2}{20} \frac{\mu_H B_x}{1+(\mu_H B_x)^2} \left\{ \mu_o n_1 n_2 \frac{4}{3} \pi h_o^3 \right\}. \qquad \text{(E30)}$$

It should be noted that the exciting coil and pickup coil may be interchanged since Onsager's reciprocity theorem states that:

$$R_{21}(B) = R_{12}(-B),$$

or

$$|R_{21}| = |R_{12}| . \qquad \text{(E31)}$$

This theorem is used to advantage in experiments where the geometry of the sample makes it easy to calculate the eddy current losses for excitation by one of the coils, and difficult to calculate for the other coil.

BIBLIOGRAPHY

Busch G., Wieland J. and Zoller H., Electrical Properties of Grey Tin, Helv. Phys. Acta., 24, 49 (1951).

Busch G., Jaggi R. and Braunschweig P., Ballistic Method for Measuring the Hall Effect, Helv. Phys. Acta., 26, 392 (1953).

Busch G. and Junod P., The Electrical Properties of Silver Selenide, Helv. Phys. Acta., 30, 470 (1957).

Dresselhaus G., Kip A. F., Kittel C. and Wagoner G., Cyclotron and Spin Resonance in Indium Antimonide, Phys. Rev., 98, 556 (1955).

Erginsoy C., Neutral Impurity Scattering in Semiconductors, Phys. Rev., 79, 1013 (1950).

Faraday M., Faraday's Diary 1820-1862, Bell and Sons, London, vol. II, p. 49.

Fischer G. and MacDonald D. K. C., Magnetoresistance and Field Dependence of the Hall Effect in Indium Antimonide, Can. J. Phys., 36, 527 (1958).

Glicksman M., The Magnetoresistivity of Germanium and Silicon, PROGRESS IN SEMICONDUCTORS, Heywood and Company, London, vol. 3, p. 1-25 (1958).

Hansen M., Constitution of Binary Alloys, McGraw-Hill, New York, 2nd Ed., p. 50 (1958).

Miyatani S., Electrical Properties of Ag_2Te, J. Phys. Soc. Japan, 13, 341 (1958).

Miyatani S., Ionic Conduction in β-Ag_2Te and β-Ag_2Se, J. Phys. Soc. Japan, 14, 996 (1959).

Prince M. B., Drift Mobilities in Semiconductors: I Germanium, Phys. Rev. 92, 681 (1953).

Stratton J. A., Electromagnetic Theory, McGraw-Hill, New York, p. 244-245 (1941).

Wait J. R., Complex Magnetic Permeability of Spherical Particles, Proc. Inst. Radio Engrs., 1664 (1953).

Wilson A. H., Theory of Metals, Cambridge University Press, 2nd Ed., Sections 8.6 - 8.64 (1954).